Open Access

Advances in Environmental and Engineering Research

LIDSEN Publishing Inc.

Original Research

Seasonal Urban Heat Persistence and Nighttime Radiance Intensification in Jaipur, India: Spatiotemporal Analysis

Rupesh Kumar Gupta [1,*], Yash Kumar Tiwari [1], Arpit Gupta [1], Grinedge Yadav [1], Swati Gupta [2,*]

1. Department of Continuing Education and Extension, Faculty of Social Sciences, University of Delhi, Delhi-110007, India; E-Mails: gisrs2004@gmail.com; phd.yash0402@gmail.com; arpitgupta2662@gmail.com; grinedge.du@gmail.com
2. Central Board of Secondary Education, New Delhi, India; E-Mail: swatigup22@gmail.com

* **Correspondences:** Rupesh Kumar Gupta and Swati Gupta; E-Mails: gisrs2004@gmail.com; swatigup22@gmail.com

Academic Editor: Grigorios L. Kyriakopoulos

Adv Environ Eng Res
2026, volume 7, issue 3
doi:10.21926/aeer.2603024

Received: April 20, 2026
Accepted: July 27, 2026
Published: August 06, 2026

Abstract

Urban thermal environments reflect the relationship between land surface temperature (LST) and anthropogenic activity. The present study analyses seasonal land surface temperature, the Urban Thermal Field Variance Index (UTFVI), and night-time radiance in Jaipur, India from 2014 to 2025 using Landsat 8 Collection 2 and VIIRS Day/Night Band datasets. The Summer (April-June) and winter (November-December) median composites were generated for continuous analysis and for classified assessment. In the study, five LST and UTFVI classes were used to examine spatial expansion with regression and correlation analyses. The mean summer LST ranged from 41.23°C to 50.62°C while winter LST varied between 19.01°C and 30.81°C. The regression results indicate interannual variability with no consistent linear warming trend over the study period. In contrast, the VIIRS radiance increased steadily from 19.06 to 26.57 nW·cm^{-2}·sr^{-1}. This result confirms sustained urban intensification. The Pearson correlation between VIIRS and summer LST was weakly negative during 2014-2018 (r = -0.286) and weaker during 2019-2025, while winter associations remained negligible. These findings indicate that increasing nighttime radiance does not directly correspond to proportional seasonal surface warming. The classified analysis shows a persistent dominance of high-summer LST classes, with extreme heat (Class 5, >45°C) accounting for more than 75% of the area in 2014 and 2019. The development of winter heat was episodic, with 2016 representing a pronounced anomaly. The UTFVI results of the study reveal sustained ecological stress with strong stress categories covering more than one-third of the urban area in most seasons. Maximum UTFVI values remained concentrated in dense built-up zones. The results of the current study demonstrate persistent summer heat, continuous radiance growth, and concentrated ecological stress in Jaipur. In the study period, the divergence between radiance expansion and LST response highlights the role of land surface composition and seasonal climate in moderating urban thermal behaviour.

Keywords

Land surface temperature; urban thermal field variance index; VIIRS nighttime radiance; seasonal thermal variability; Google Earth Engine; Jaipur

1. Introduction

Urbanisation modifies land-surface properties and alters the surface energy balance. Built-up materials, such as concrete and asphalt, increase heat storage capacity and reduce evapotranspiration. As vegetation cover declines, latent heat flux decreases and the sensible heat flux increases. These processes lead to elevated land surface temperature (LST) in urban cores compared with surrounding rural areas. This phenomenon is widely pronounced as the urban heat island effect [1]. Thermal remote sensing has become central to assessing urban heat. The input for spatially continuous measurements that allow comparison across cities and over long periods is provided by Satellite-derived LST [2, 3]. Several studies confirm that the Landsat missions have been widely used due to their moderate spatial resolution and long historical archive, as well as retrieval methods, such as the mono-window and split-window algorithms [4-6]. The calibration and radiometric correction procedures for Landsat sensors have also been standardized, and these developments allow reliable inter-annual comparison of thermal patterns.

Several studies have examined LST patterns in Indian cities using Landsat data, reporting that the relationship between LST and impervious-surface fraction or vegetation indices holds across multiple regional contexts [7-9]. The summer conditions typically amplify thermal contrasts due to reduced soil moisture and sparse vegetation cover as shown by the seasonal temperature analysis and similar patterns have been observed in semi-arid urban regions [9]. Past studies focus on short time intervals or a single reference year, but long-term assessment is essential for understanding persistent warming trends and adding value to the study. The radiometric performance and data continuity for terrestrial thermal monitoring are improved by the Landsat-8 data [10]. Consistent LST derivation methods enable multi-year comparisons and trend estimation; further analysis allows identification of the gradual expansion of high-temperature zones and quantification of thermal acceleration rates [11, 12].

Urban heat is not only expressed in terms of temperature magnitude, but it also reflects spatial thermal stress relative to background conditions. The urban thermal field variance index (UTFVI) measures the deviation of pixel-level temperature from the mean urban temperature, providing an indicator of ecological stress intensity [13]. The UTFVI index has been applied to assess environmental pressure in rapidly urbanising regions across the globe. Several studies in Ethiopia and India demonstrate that strong UTFVI classes often correspond to dense built-up clusters and low vegetation cover [11, 14]. The seasonal variations in UTFVI reflect differences in various environmental aspects such as atmospheric moisture, solar radiation, and surface characteristics [8, 11]. The integration of LST and UTFVI provides both absolute and relative measures of thermal conditions.

The UTFVI is used to identify heat hotspots and ecological stress zones suggested by recent research in Indian metropolitan areas [12, 13]. These analyses reveal expansion of high-stress classes in response to urban densification, though most investigations are limited to two or three benchmark years. The annual evaluation remains limited, particularly for medium-sized cities in semi-arid regions (Jaipur). Anthropogenic activity contributes to urban thermal conditions through energy consumption, transportation, industrial activity, and artificial lighting. The Nighttime light data from the Visible Infrared Imaging Radiometer Suite (VIIRS) Day/Night Band provides a spatial proxy for human activity intensity [15]. The VIIRS data offer improved radiometric sensitivity compared with earlier used DMSP-OLS sensors [16].

The VIIRS data have been widely used to estimate economic activity, population distribution, and urban expansion [17-19] because calibration refinements and cross-sensor harmonization improve temporal consistency [20, 21]. The long-term VIIRS datasets enable evaluation of anthropogenic growth patterns over decadal scales [22]. The artificial light distribution also reflects the spatial concentration of infrastructure and built-up intensity [23]. Multi-temporal VIIRS observations have revealed anisotropic and directional characteristics of artificial lighting [24]. Several studies have demonstrated that nighttime radiance correlates with impervious surface density and urban core expansion [17, 25]. Recent research has begun to explore the relationship between nighttime radiance and urban thermal patterns. Although several studies have reported positive associations between nighttime radiance and elevated land surface temperature, the strength and direction of this relationship vary considerably across cities and climatic regions because urban thermal behavior is simultaneously controlled by vegetation, land-cover composition, urban morphology, soil moisture, and seasonal atmospheric conditions [26]. Such findings suggest that anthropogenic intensity may reinforce thermal anomalies. The systematic seasonal analysis linking VIIRS, LST, and ecological stress indices remains limited. Most existing urban heat studies focus on large metropolitan regions. The medium-sized cities in semi-arid India are less frequently examined despite rapid spatial transformation. Jaipur has experienced steady population growth and outward urban expansion during the past decade. Land-cover conversion and densification have modified its surface thermal structure. Previous work in Indian cities has examined relationships between LST and built-up indices [6, 7]. Some studies have incorporated UTFVI to evaluate ecological stress [11-15]. Nighttime radiance has been used to analyse economic growth and infrastructure intensity [16, 17]. However, integration of these three components within a continuous seasonal framework remains limited. Although nighttime radiance is widely recognised as an effective proxy for urbanisation intensity and anthropogenic activity, its relationship with land surface temperature (LST) is neither linear nor spatially uniform. Urban thermal behaviour is governed by the surface energy balance, which reflects the combined influence of incoming solar radiation, surface albedo, thermal inertia, evapotranspiration, aerodynamic properties, and anthropogenic heat emissions. Consequently, areas exhibiting high nighttime radiance do not necessarily experience proportionally higher daytime surface temperatures because multiple environmental and morphological factors regulate heat storage and dissipation [27].

Vegetation plays a particularly important moderating role by reducing surface temperature through evapotranspiration and shading. Urban green spaces, irrigated landscapes, and peri-urban vegetation can substantially reduce LST even within highly illuminated urban environments. Similarly, soil moisture influences the partitioning of available energy into latent and sensible heat fluxes, thereby limiting surface heating despite increasing urban development. Seasonal variability further modifies these interactions, especially in semi-arid environments where rainfall, atmospheric humidity, and antecedent moisture conditions fluctuate considerably between years.

Urban morphology introduces an additional level of complexity. High-rise buildings, compact street canyons, varying building densities, and differences in construction materials alter solar exposure, shadow patterns, wind circulation, and heat storage capacity. Consequently, two locations with similar nighttime radiance may exhibit substantially different thermal responses depending on their urban form and land-cover composition. Modern urban developments may also incorporate reflective roofing materials, landscaped open spaces, and improved building designs that partially offset surface warming despite increasing anthropogenic activity.

Recent studies increasingly suggest that nighttime light intensity should not be interpreted as a direct surrogate for urban thermal conditions but rather as one component of a more complex urban environmental system [28, 29]. The interaction among vegetation dynamics, land-cover composition, surface moisture availability, urban morphology, and climatic variability often produces nonlinear relationships between anthropogenic radiance and land surface temperature. Understanding these moderating mechanisms is therefore essential for interpreting apparent decoupling between urban expansion and thermal response, particularly in rapidly growing semi-arid cities such as Jaipur.

Few studies assess both summer and winter patterns within the same year over an extended period, but the seasonal differentiation is important in semi-arid climates where thermal amplitude varies significantly across months [30]. The continuous annual assessment from 2014 onward is feasible due to consistent Landsat-8 coverage and stable VIIRS observations [2, 14]. Recent urban climate research has increasingly shifted from simple urban heat island mapping towards integrated assessments that combine land surface temperature, vegetation dynamics, nighttime light observations, ecological stress, and climate resilience [31]. Contemporary studies emphasise that urban thermal environments are regulated by the interaction of land-use change, urban morphology, vegetation cover, and climatic variability rather than by a single environmental indicator [32, 33]. Recent applications of VIIRS nighttime light data demonstrate that anthropogenic radiance is a valuable proxy for urbanisation intensity but should be interpreted alongside land surface characteristics to better understand thermal behaviour and sustainable urban development. These advances highlight the importance of integrated, long-term satellite-based assessments, particularly for rapidly expanding semi-arid cities where seasonal climatic variability strongly influences urban thermal dynamics. This study evaluates the spatiotemporal dynamics of LST and ecological thermal stress in Jaipur during 2014-2025. The seasonal analysis is conducted for summer (April-June) and winter (November-December) of each year. The annual VIIRS nighttime radiance is incorporated to examine the association between anthropogenic intensity and surface thermal conditions. An integrated understanding of urban heat development has been assessed using continuous trends and classified spatial expansion.

2. Materials and Methods

2.1 Study Area

Jaipur is located in the eastern part of Rajasthan, India. It is situated between approximately 26°45′-27°05′ N latitude and 75°40′-76°00′ E longitude (Figure 1). The city lies within a semi-arid climatic zone. The city is characterised by high summer temperatures and low annual precipitation. The elevation ranges from approximately 430 m to 480 m above mean sea level. A significant part of the Aravalli hill system influences local topography and wind movement in Jaipur. The climate of Jaipur shows marked seasonal contrast; summer spans from April to June with intense heat and low humidity. The surface temperatures frequently exceed 40°C during this period, while the winter conditions in November and December are comparatively mild with reduced solar intensity and lower mean temperatures. This kind of seasonal contrast makes Jaipur suitable for evaluating intra-annual thermal variation.

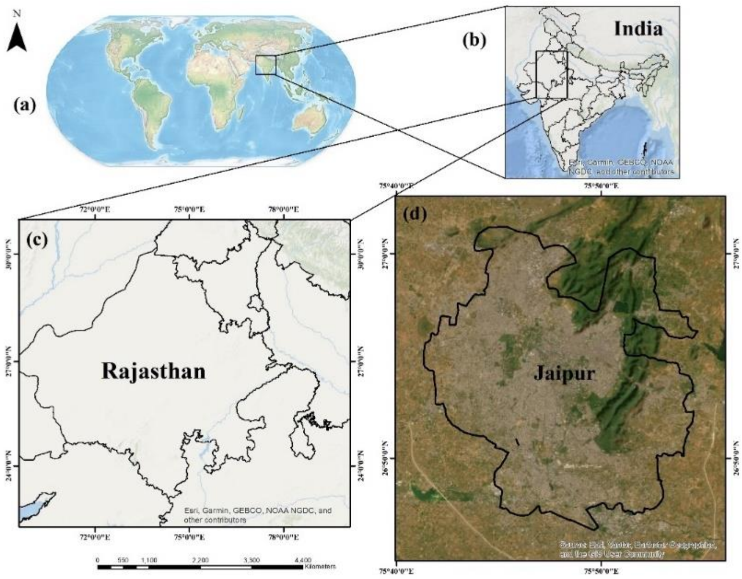

Figure 1 Location map of the study Area (a) Location of the Indian Subcontinent in the world; (b) Location of India in the Indian Subcontinent; (c) Location of Rajasthan; (d) Location of Jaipur.

Over the last decade, the urban expansion in Jaipur has accelerated. The marginal agricultural land has gradually been converted into residential and commercial built-up areas. The increased impervious surface fraction contributes to enhanced surface heat retention in the urban areas of Jaipur. Several studies have shown that impervious surfaces correlate strongly with elevated land-surface temperatures [34]. In multiple Indian urban environments, the vegetation indices show inverse relationships with LST [35, 36]. The urban heat patterns in Jaipur are rapidly expanding cities influenced by land-cover change and infrastructure concentration [37]. The semi-arid settings with sparse vegetation cover are particularly sensitive to such transformation. The administrative boundary of Jaipur Municipal Corporation was used as the study extent. All spatial statistics and temporal analyses were confined to this boundary. Jaipur signifies a semi-arid urban system for examining seasonal thermal magnitude, ecological stress intensity, and anthropogenic radiance patterns over a continuous multi-year period.

2.2 Satellite Datasets

The Landsat 8 and Landsat 9 Collection 2 Level 2 surface temperature products were used to derive the LST. The Landsat 8 provides 30 metre spatial resolution with improved radiometric performance and long-term continuity [2]. The calibration procedures and radiometric coefficients are documented in detail by Chander et al. [5]. The Collection 2 products incorporate atmospheric correction and emissivity handling within the surface temperature band. The analysis period for the study covers 2014-2025, ensuring consistency of Landsat 8 observations and stable VIIRS data availability [14, 15]. The seasonal composites were generated for Summer (April-June) and Winter (November-December) for each year. The median composites were created to reduce the influence of cloud contamination and short-term atmospheric variability.

After applying standard cloud masking procedures to Landsat data [38], nighttime radiance was derived from VIIRS Day/Night Band monthly cloud-free composites (VCMSLCFG). The VIIRS provides a higher dynamic range and better sensitivity than earlier used DMSP-OLS sensors. The improved calibration and cross-sensor harmonisation have also enhanced temporal consistency, making the dataset suitable for long-term trend analysis for the study area. The annual mean radiance composites were calculated for each year for the study area, and all spatial processing was conducted using Google Earth Engine to ensure uniform preprocessing and reproducibility.

2.3 Land Surface Temperature Derivation

Surface temperature was extracted from the thermal infrared band (ST_{B10}) of Landsat Collection 2 Level 2 products. The scale factor and additive offset provided in the metadata were applied (eq. 1).

The conversion to degrees Celsius followed:

$$LST(°\mathrm{C}) = (ST_{B10} \times 0.00341802 + 149) - 273.15 \tag{1}$$

This transformation converts scaled digital values to surface temperature in Kelvin and subsequently to Celsius. The methodological basis for thermal retrieval and emissivity correction is described in Li et al. [4] and Roy et al. [2]. Seasonal median composites were calculated separately for each year to represent representative summer and winter thermal conditions.

2.4 Urban Thermal Field Variance Index

Ecological thermal stress was evaluated using the urban thermal field variance index (UTFVI). UTFVI expresses the relative deviation of pixel-level temperature from the mean seasonal temperature of the study area (eq. 2).

$$UTFVI = \frac{T_s - T_{mean}}{T_{mean}} \tag{2}$$

where:
T_s = pixel-level land surface temperature.
T_{mean} = mean seasonal land surface temperature of Jaipur.

UTFVI provides a normalised measure of thermal stress [39]. Higher values indicate stronger deviation from background temperature and greater ecological pressure [40, 41]. For each season and year, UTFVI was computed from the corresponding LST composite.

2.5 Classification Scheme

Continuous LST and UTFVI values were classified into five categories to examine spatial expansion patterns.

2.5.1 Seasonal LST Classification

Separate thresholds were defined for summer and winter to account for climatic differences. This approach allows inter-annual comparison within each season (Table 1 and Table 2).

Table 1 Summer LST classification thresholds.

Class	Temperature range (°C)	Interpretation
1	<35	Very low
2	35-40	Low
3	40-45	Moderate
4	45-48	High
5	>48	Very high

Table 2 Winter LST classification thresholds.

Class	Temperature range (°C)	Interpretation
1	<18	Very low
2	18-22	Low
3	22-25	Moderate
4	25-28	High
5	>28	Very high

Season-specific thresholds avoid artificial comparison between summer and winter magnitudes and focus on intra-seasonal trend evaluation.

2.5.2 UTFVI Classification

UTFVI values were classified following established ecological stress categories (Table 3).

Table 3 UTFVI classification thresholds.

Class	UTFVI range	Ecological condition
1	≤0	No stress
2	0-0.005	Weak stress
3	0.005-0.01	Moderate stress
4	0.01-0.015	Strong stress
5	>0.015	Very strong stress

This classification enables assessment of the spatial expansion of high-stress zones over time. The "No Stress" UTFVI class represents pixels with land surface temperatures at or below the seasonal mean, indicating relatively lower thermal stress within the study area rather than the complete absence of heat. As UTFVI is a relative index derived from the deviation of pixel temperature from the seasonal mean, the classification reflects comparative ecological thermal conditions across the study area rather than absolute temperature levels.

2.6 Area Statistics

The area of each class was calculated using pixel area conversion. Pixel area in square kilometres was obtained as (eq. 3):

$$Area(km^2) = Pixel\ Area(m^2) \div 10^6 \tag{3}$$

Total area per class was calculated by summing pixel areas within each class. The percentage area was derived as (eq. 4):

$$Area\ \% = \frac{Area\ class}{Total\ area} \times 100 \tag{4}$$

This procedure was implemented in Google Earth Engine using grouped reduction functions.

2.7 Relationship with Nighttime Radiance

Annual mean VIIRS radiance values were extracted for the study area. Pearson correlation coefficient (r) was calculated as (eq. 5):

$$r = \frac{\sum(X - \bar{X})(Y - \bar{Y})}{\sqrt{\sum(X - \bar{X})^2 \sum(Y - \bar{Y})^2}} \tag{5}$$

where:
X = annual VIIRS radiance.
Y = annual mean LST or UTFVI.

Linear regression between VIIRS and thermal indicators was also estimated. This method has been used in previous studies to explore the links between nighttime radiance and urban thermal situations [42-44]. Linear regression was applied as a descriptive statistical tool to examine the overall direction of temporal relationships among the variables. The analysis was not intended to represent the full complexity of climatic trend detection or non-linear environmental variability.

2.8 Ethics Statement

This study used publicly available satellite remote sensing datasets, including Landsat Collection 2 Level 2 products and VIIRS Day/Night Band composites. All data were obtained from open-access platforms and contain no individual-level or personally identifiable information. In the current study, no human participants, animal subjects, or plant specimens were directly involved. The analysis was conducted at the city scale using aggregated spatial data. Therefore, institutional ethical approval and informed consent were not required.

3. Results

3.1 Mean Seasonal Land Surface Temperature, UTFVI and VIIRS Radiance (2014-2025)

The interannual variation of seasonal mean LST, UTFVI, and annual VIIRS radiance for 2014-2025 is presented in Table 4. Summer LST ranged from 41.23°C (2023) to 50.62°C (2019). The elevated summer temperatures were recorded in 2014 (47.07°C) and 2019 (50.62°C), while relatively moderate values occurred in 2016 (44.96°C), 2021 (45.13°C) and 2022 (45.95°C). A distinct decline in 2023 (41.23°C) followed by a recovery in 2024 (47.59°C). The winter LST ranged between 19.01°C (2019) and 30.81°C (2016) (Figure 2 and Figure 3). The winter peak during 2015-2016 reflects anomalous warm-season behaviour consistent with earlier urban thermal observations in semi-arid Indian cities. The annual VIIRS radiance increased steadily after 2014, rising from 19.06 to 26.57 $nW \cdot cm^{-2} \cdot sr^{-1}$ in 2025. The growth pattern is monotonic, indicating sustained anthropogenic intensification. The strong radiance increases the contrast with the weak temporal trend in LST, suggesting that the thermal response is modulated by land-cover composition and seasonal climate variability rather than by light intensity alone (Figure 4). The mean UTFVI values remained close to zero throughout the study period because the index is calculated relative to the seasonal mean land surface temperature. Consequently, the ecological significance of UTFVI is better represented by its spatial distribution and class composition than by temporal variations in the mean values. To facilitate consistent temporal comparison across all study years, a uniform grayscale classification scheme has been maintained for the classified LST and UTFVI maps (Figures 5-9). This approach enables clearer visual identification of changes in the spatial extent and persistence of thermal classes, while the corresponding-coloured maps provide complementary visualisation of the seasonal thermal patterns.

Table 4 Mean seasonal land surface temperature (°C), mean UTFVI, and annual VIIRS radiance ($nW \cdot cm^{-2} \cdot sr^{-1}$) for Jaipur (2014-2025).

Year	Summer LST (°C)	Winter LST (°C)	Summer UTFVI	Winter UTFVI	VIIRS radiance
2014	47.07	28.08	1.57E-14	5.05E-15	19.06
2015	47.68	30.07	3.42E-14	-1.61E-14	19.85
2016	44.96	30.81	-3.82E-14	6.56E-15	19.96
2017	46.21	28.11	-1.92E-15	6.79E-15	19.51
2018	47.85	26.89	1.56E-14	-3.35E-14	20.13
2019	50.62	19.01	2.70E-14	-4.92E-14	21.03
2020	45.82	26.81	9.53E-15	-2.75E-14	20.60
2021	45.13	26.23	-2.79E-14	-6.40E-14	21.90
2022	45.95	27.17	-1.58E-14	3.44E-14	21.96
2023	41.23	26.50	-3.70E-14	-5.45E-15	24.28
2024	47.59	28.53	3.28E-15	-1.85E-14	26.13
2025	45.02	26.52	2.33E-14	-3.57E-14	26.57

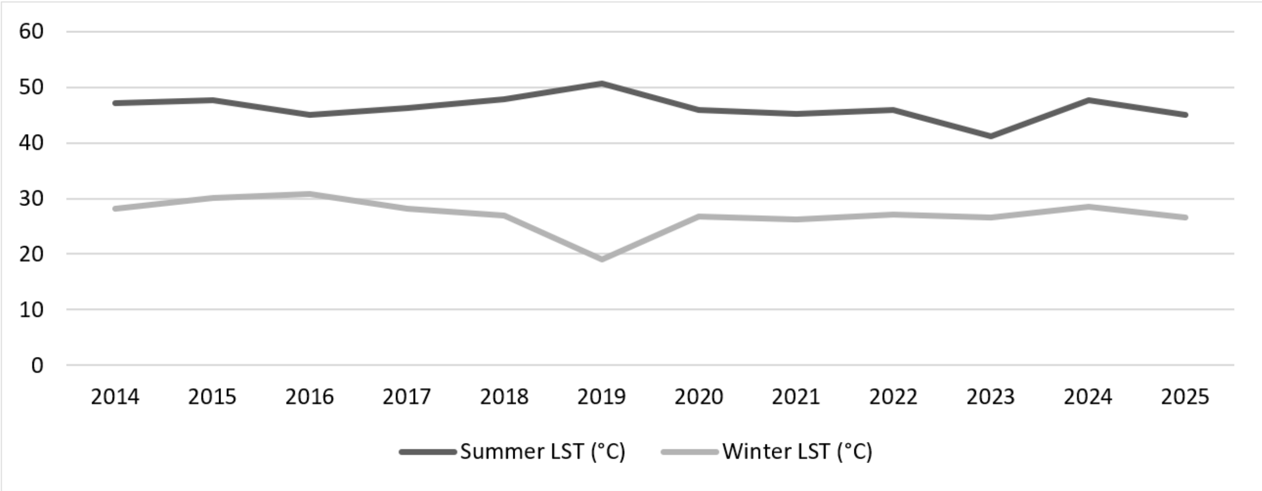

Figure 2 Interannual variation of mean summer and winter LST (2014-2025).

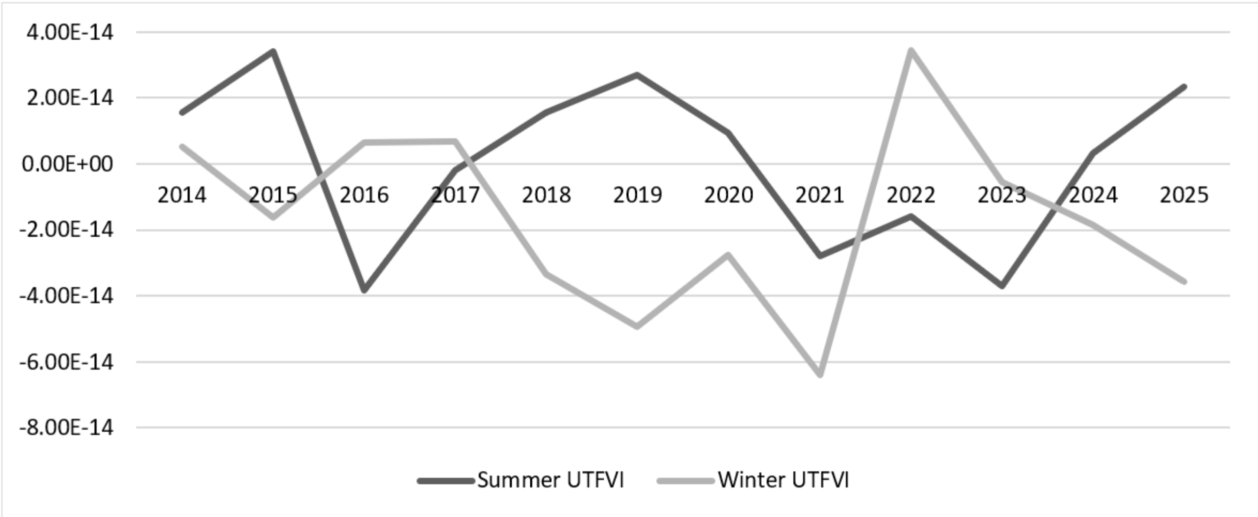

Figure 3 Interannual variation of mean summer and winter UTFVI (2014-2025).

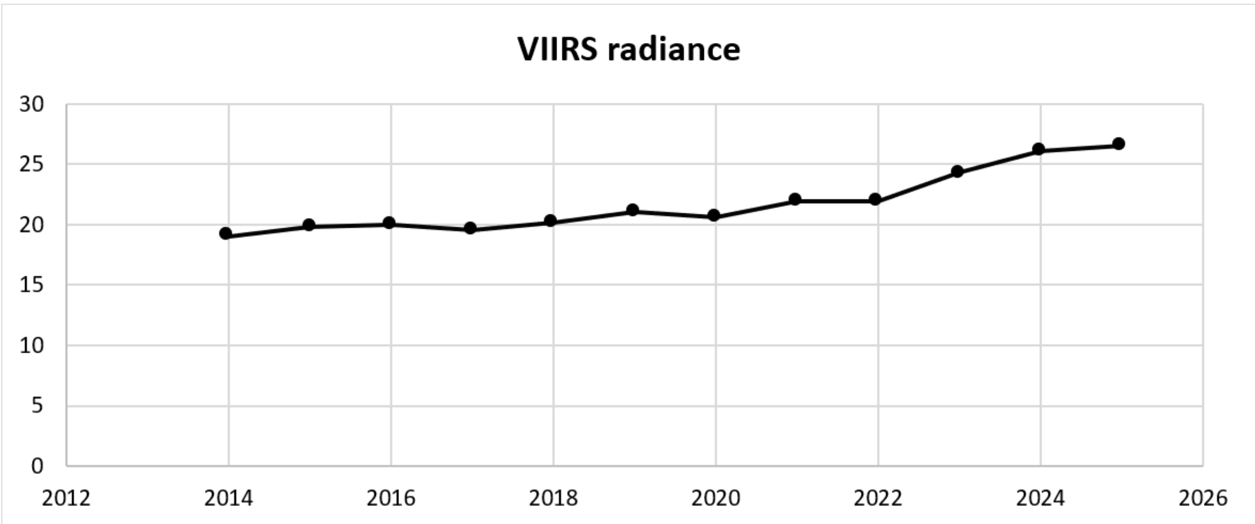

Figure 4 Interannual variation of VIIRS nighttime (2014-2025).

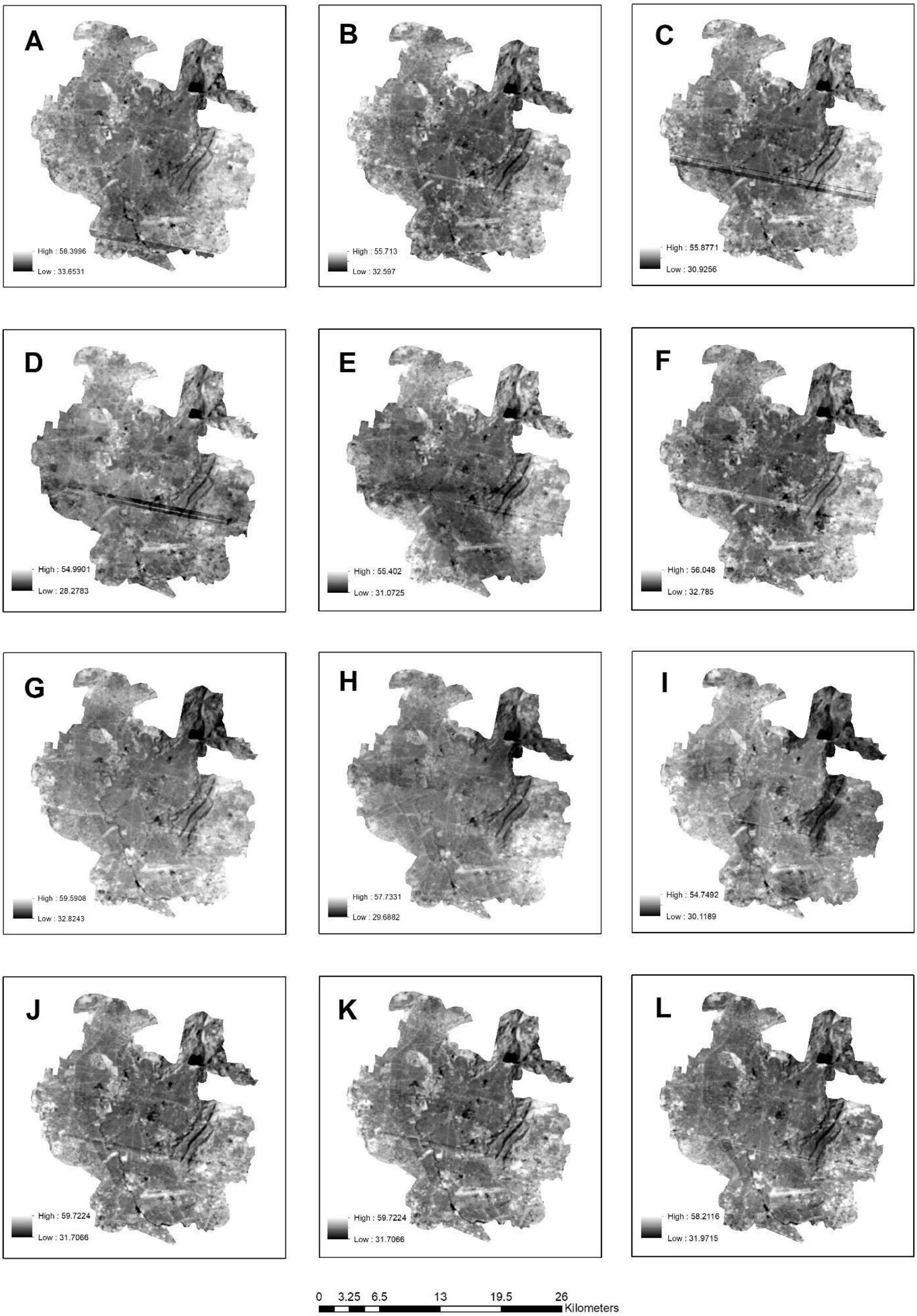

Figure 5 Spatial distribution of summer LST for the years 2014-2025, respectively.

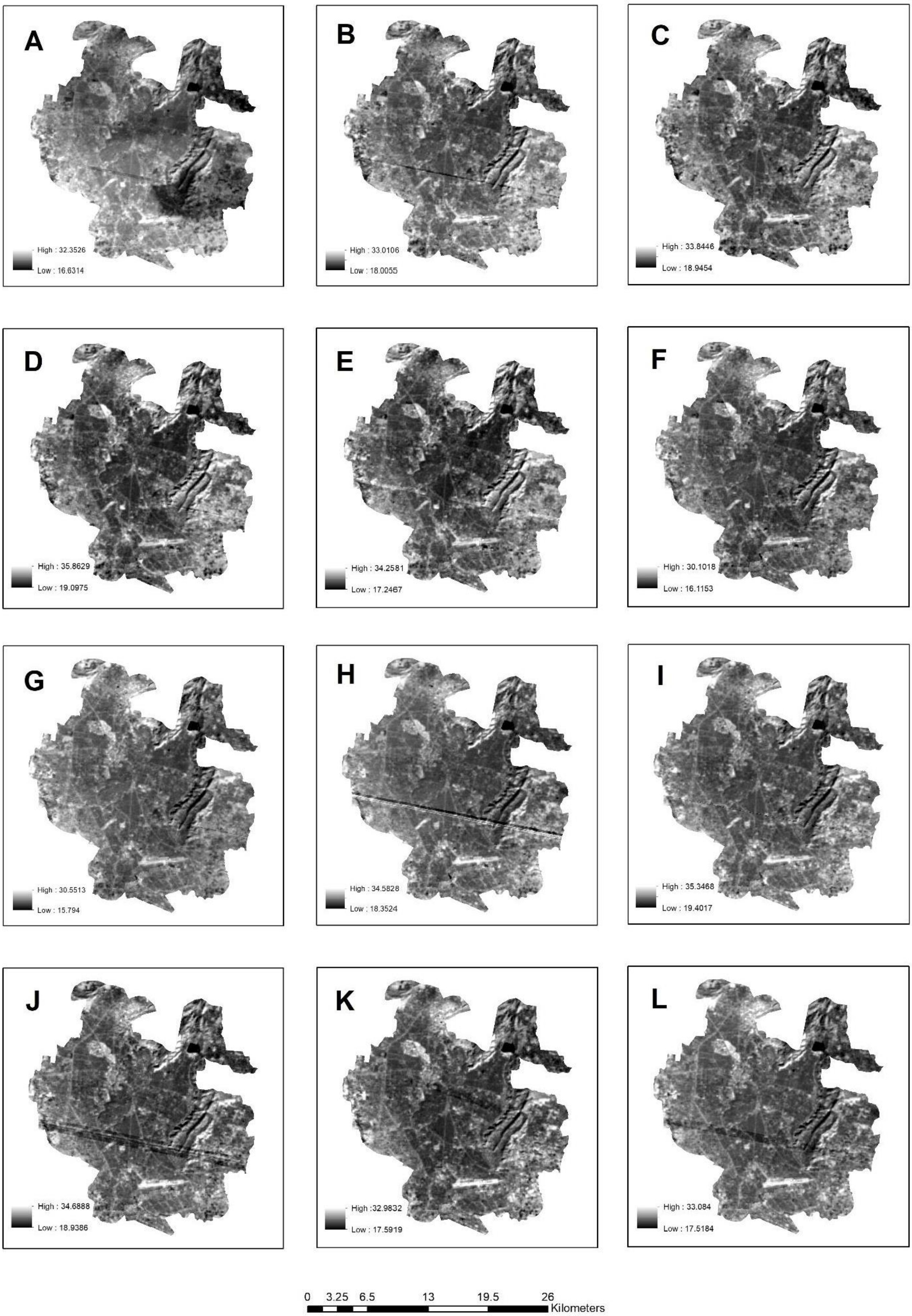

Figure 6 Spatial distribution of winter LST for the years 2014-2025, respectively.

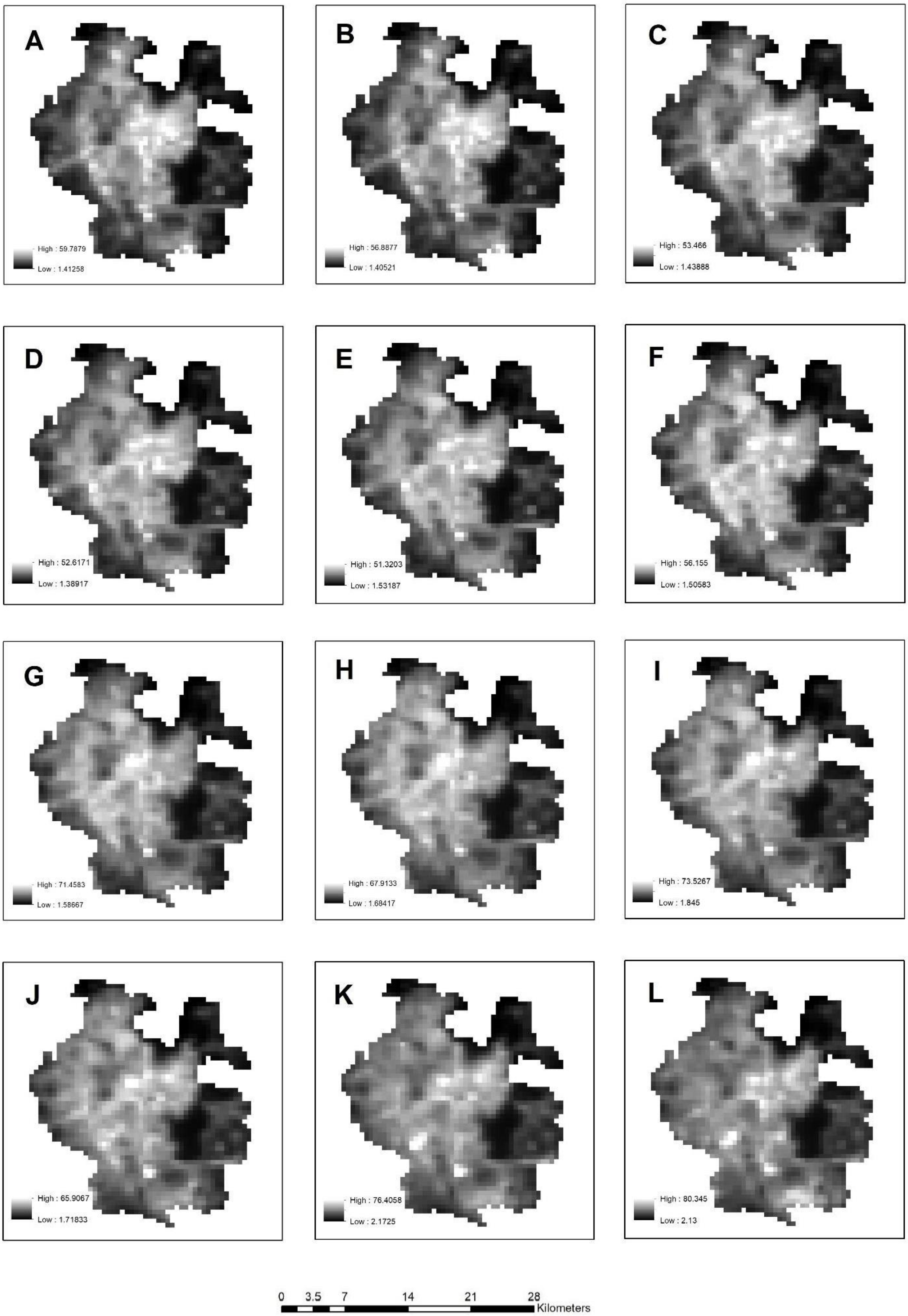

Figure 7 Spatial distribution of VIIRS for the years 2014-2025, respectively.

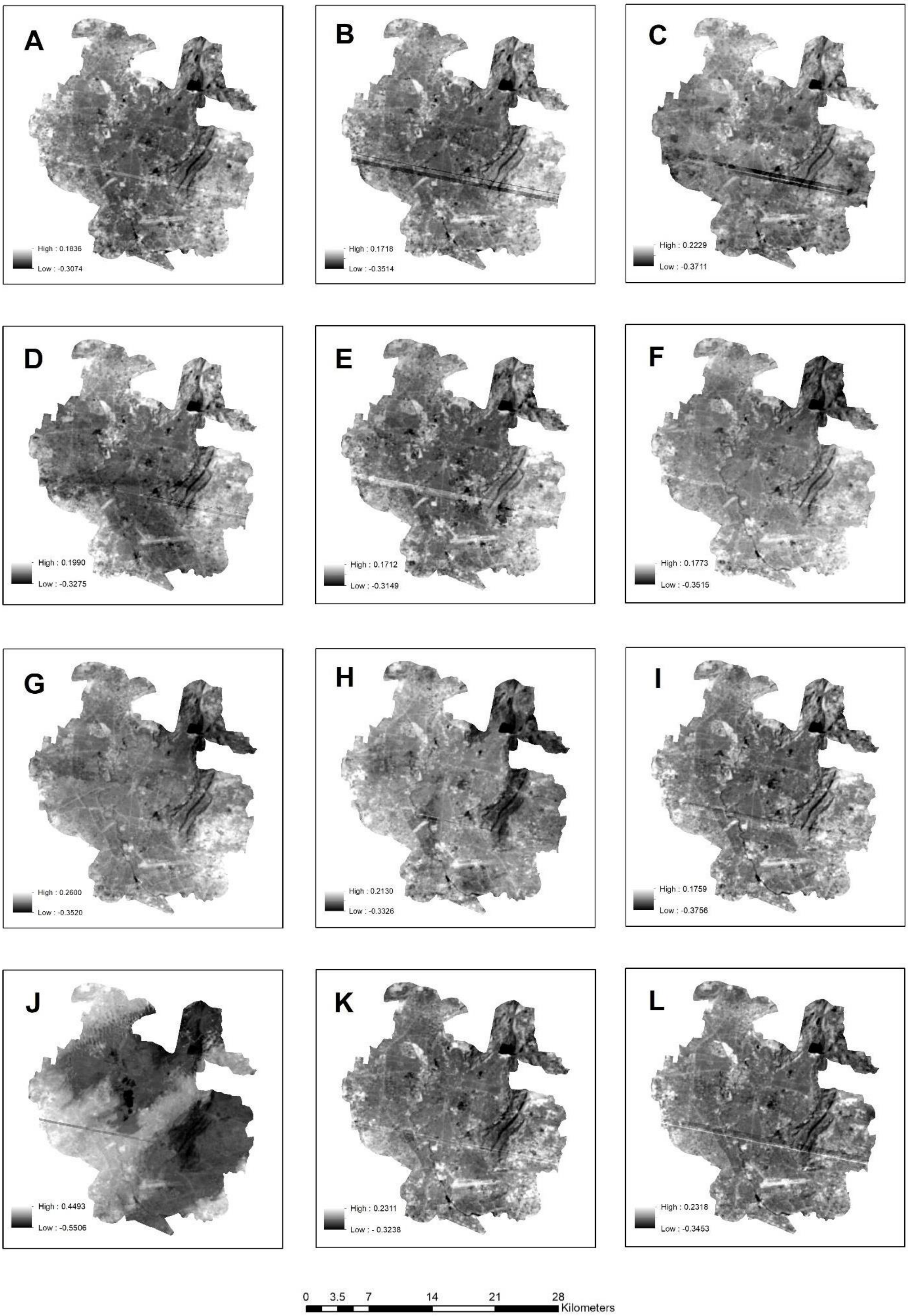

Figure 8 Spatial distribution of Summer UTFVI for the years 2014-2025, respectively.

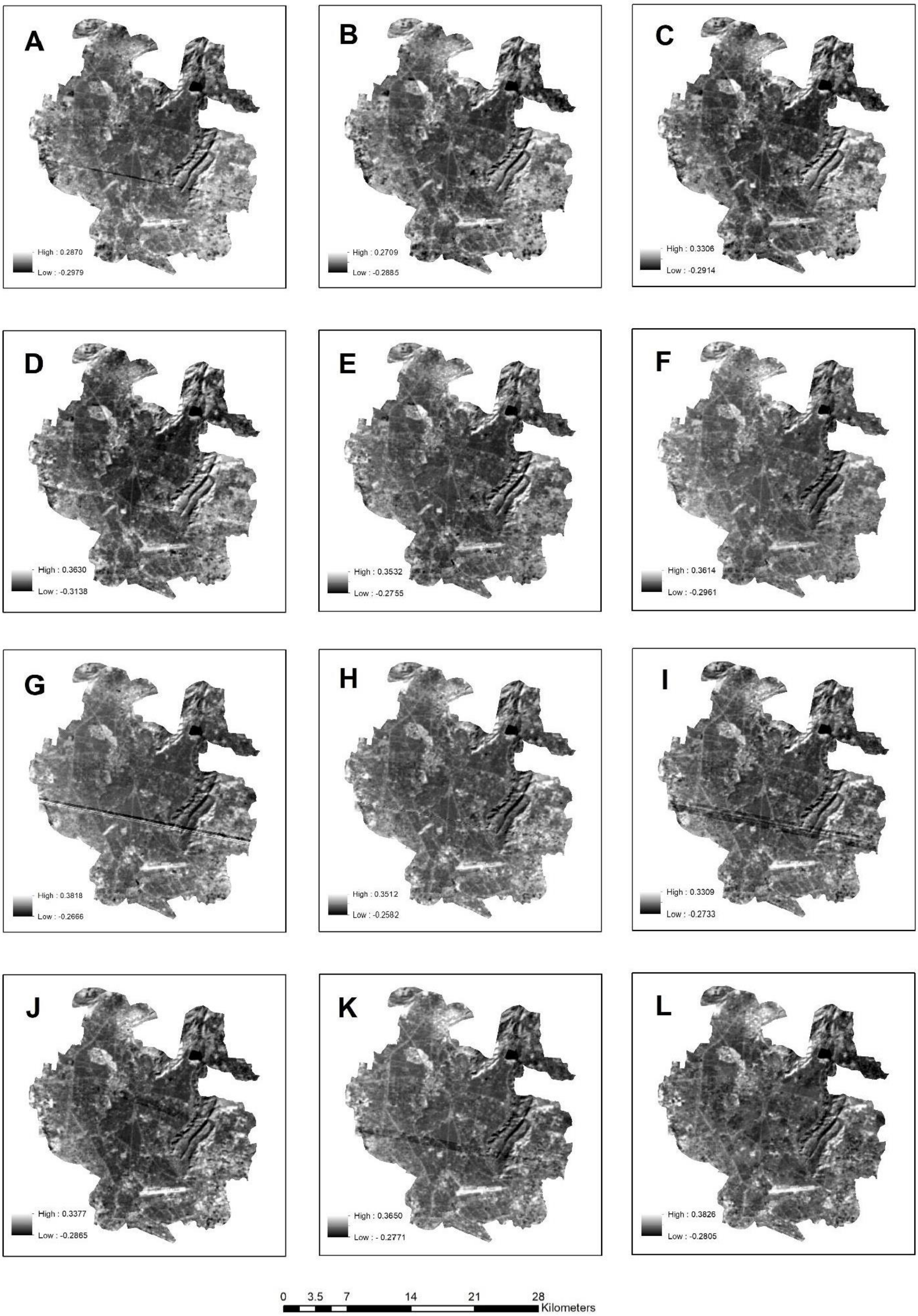

Figure 9 Spatial distribution of Winter UTFVI for the years 2014-2025.

3.2 Correlation and Regression Statistics (2014-2025)

Regression analysis shows weak temporal trends in seasonal LST (Table 5). Summer LST exhibits a slight negative slope (-0.23°C per year; R^2 = 0.082). Winter LST shows even weaker association with time (R^2 = 0.009) (Figure 10). These results indicate that seasonal mean land surface temperature does not exhibit a strong linear temporal trend during the study period. The regression analysis was used to provide a descriptive assessment of temporal variability. It should not be interpreted as evidence of the complete climatic behaviour, which may involve non-linear fluctuations and interannual variability. The VIIRS radiance shows a strong linear trend with year (R^2 = 0.867) (Figure 11), confirming a sustained expansion of illuminated surfaces and built-up infrastructure.

Table 5 Pearson correlation coefficients, regression slopes, and R^2 values between year, VIIRS radiance, and seasonal LST (2014-2025).

Relationship	Pearson r	Direction	Regression slope	R^2
VIIRS vs Summer LST	-0.286	Weak negative	-0.23°C per radiance unit	0.082
VIIRS vs Winter LST	0.183	Weak positive	0.15°C per radiance unit	0.033
Year vs VIIRS	0.931	Strong positive	+0.63 radiance per year	0.867
Year vs Summer LST	-0.278	Weak negative	-0.25°C per year	0.077
Year vs Winter LST	-0.096	Very weak negative	-0.07°C per year	0.009

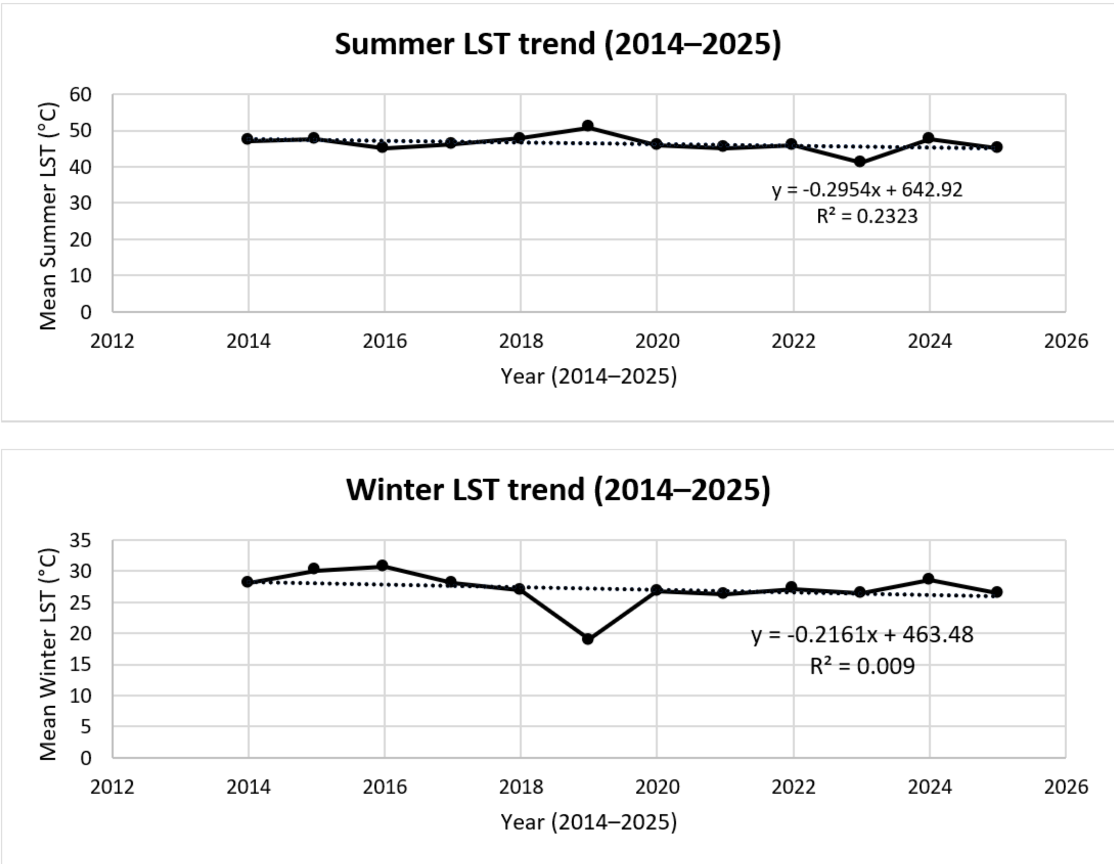

Figure 10 Linear regression of year versus summer and winter LST.

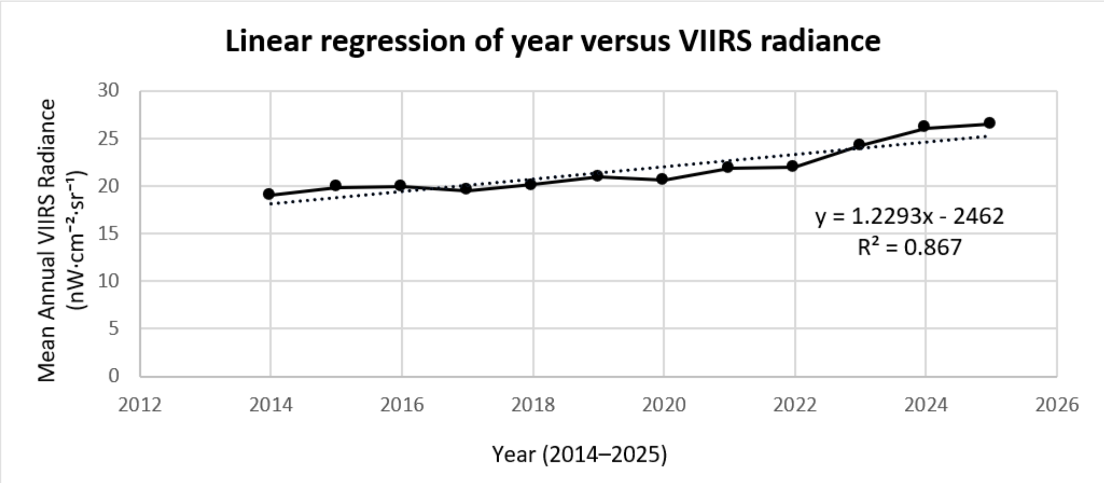

Figure 11 Linear regression of year versus VIIRS radiance.

The relationship between VIIRS and seasonal LST remains weak to moderate. The VIIRS versus summer LST shows a moderate negative association (R^2 = 0.082) (Figure 12), whereas VIIRS versus winter LST shows a very weak association (R^2 = 0.033) (Figure 13). This suggests that increased nighttime radiance does not translate directly into proportional daytime surface heating at the city scale. Urban thermal response depends on impervious surface fraction, vegetation cover, and seasonal meteorology. Year vs VIIRS shows a strong positive association (R^2 = 0.867) (Figure 11). Radiance increased steadily during the period. Year vs LST relationships are weak. This indicates that seasonal surface temperature does not follow a simple linear trajectory. VIIRS vs Summer LST shows a moderate negative association. VIIRS vs Winter LST is weak. Anthropogenic light growth does not directly translate to uniform surface warming. Similar weak relationships have been reported in Indian cities.

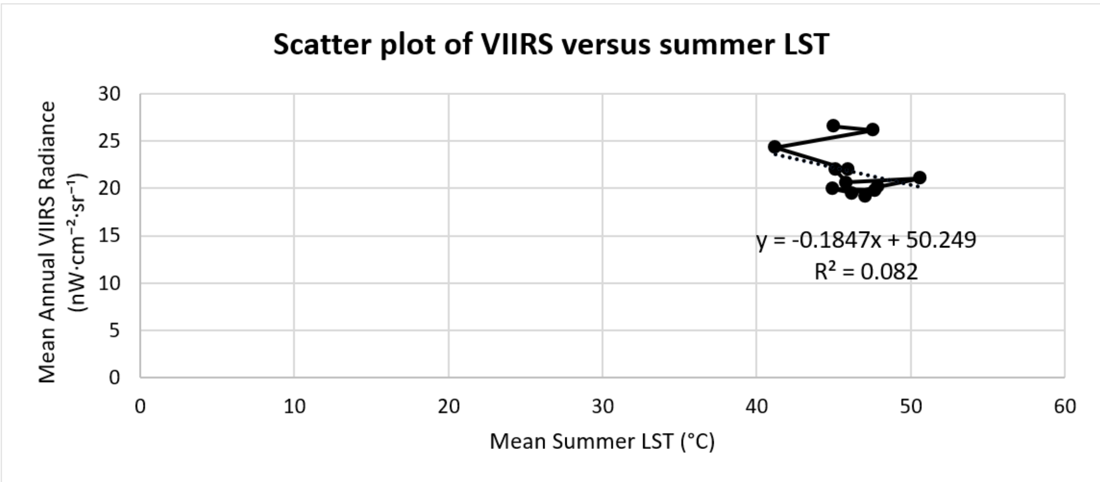

Figure 12 Scatter plot of VIIRS versus summer LST.

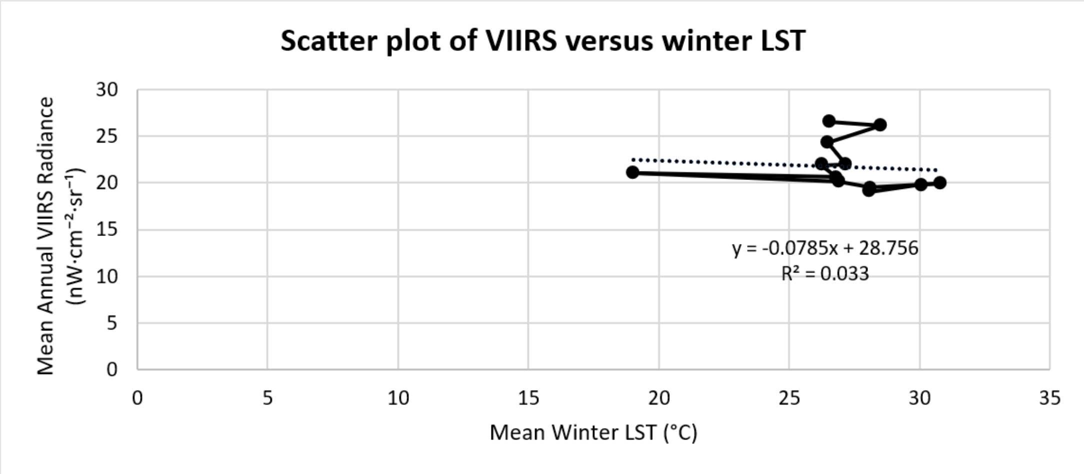

Figure 13 Scatter plot of VIIRS versus winter LST.

3.3 Classified Summer LST Area Distribution (2014-2025)

The summer LST classification reveals dominance of higher thermal classes across multiple years (Table 6) (Figure 14). In 2014, Class 5, which indicates >48 degrees, covered 130.20 km^2 (34.61%), increasing to 321.93 km^2 (85.57%) in 2019. These years correspond to peak mean summer LST. In contrast, 2016 and 2023 show redistribution towards moderate categories. In 2016, Class 3, which indicates 40-45°C, occupied 194.37 km^2 (51.66%). In 2023, Class 3 (40-45°C) expanded to 208.13 km^2 (55.32%), while Class 5 (above 48°C) declined sharply to 4.85 km^2 (1.29%). This shift reflects interannual climatic variability and possible monsoonal moderation during composite months. The classes below 35°C and 35-40°C consistently occupied less than 5% of the total area in most years. The dominance of Classes 4 (45-48°C) and 5 (Above 48°C) confirms the persistence of summer thermal stress within the urban core. Comparable spatial concentration of extreme summer heat has been reported in Indian semi-arid cities.

Table 6 Summer LST class area (km^2 and %), 2014-2025.

Year	Below 35°C		35-40°C		40-45°C		45-48°C		Above 48°C	
	km^2	%	km^2	%	km^2	%	km^2	%	km^2	%
2014	0.74	0.20	1.00	0.27	78.04	20.74	166.23	44.19	130.20	34.61
2015	0.86	0.23	0.81	0.21	49.96	13.28	162.48	43.19	162.10	43.09
2016	0.68	0.18	5.82	1.55	194.37	51.66	141.82	37.70	33.53	8.91
2017	0.72	0.19	1.63	0.43	136.38	36.25	137.72	36.61	99.77	26.52
2018	0.63	0.17	0.75	0.20	39.70	10.55	166.11	44.15	169.03	44.93
2019	0.57	0.15	0.49	0.13	10.06	2.67	43.16	11.47	321.93	85.57
2020	1.06	0.28	9.48	2.52	136.29	36.23	151.66	40.31	77.73	20.66
2021	1.00	0.27	14.96	3.98	150.42	39.98	167.32	44.47	42.53	11.30
2022	0.95	0.25	1.25	0.33	137.99	36.68	164.66	43.77	71.36	18.97
2023	11.23	2.99	120.17	31.94	208.13	55.32	31.83	8.46	4.85	1.29
2024	0.92	0.24	0.91	0.24	49.59	13.18	170.10	45.21	154.69	41.12
2025	0.91	0.24	3.54	0.94	193.26	51.37	144.47	38.40	34.04	9.05

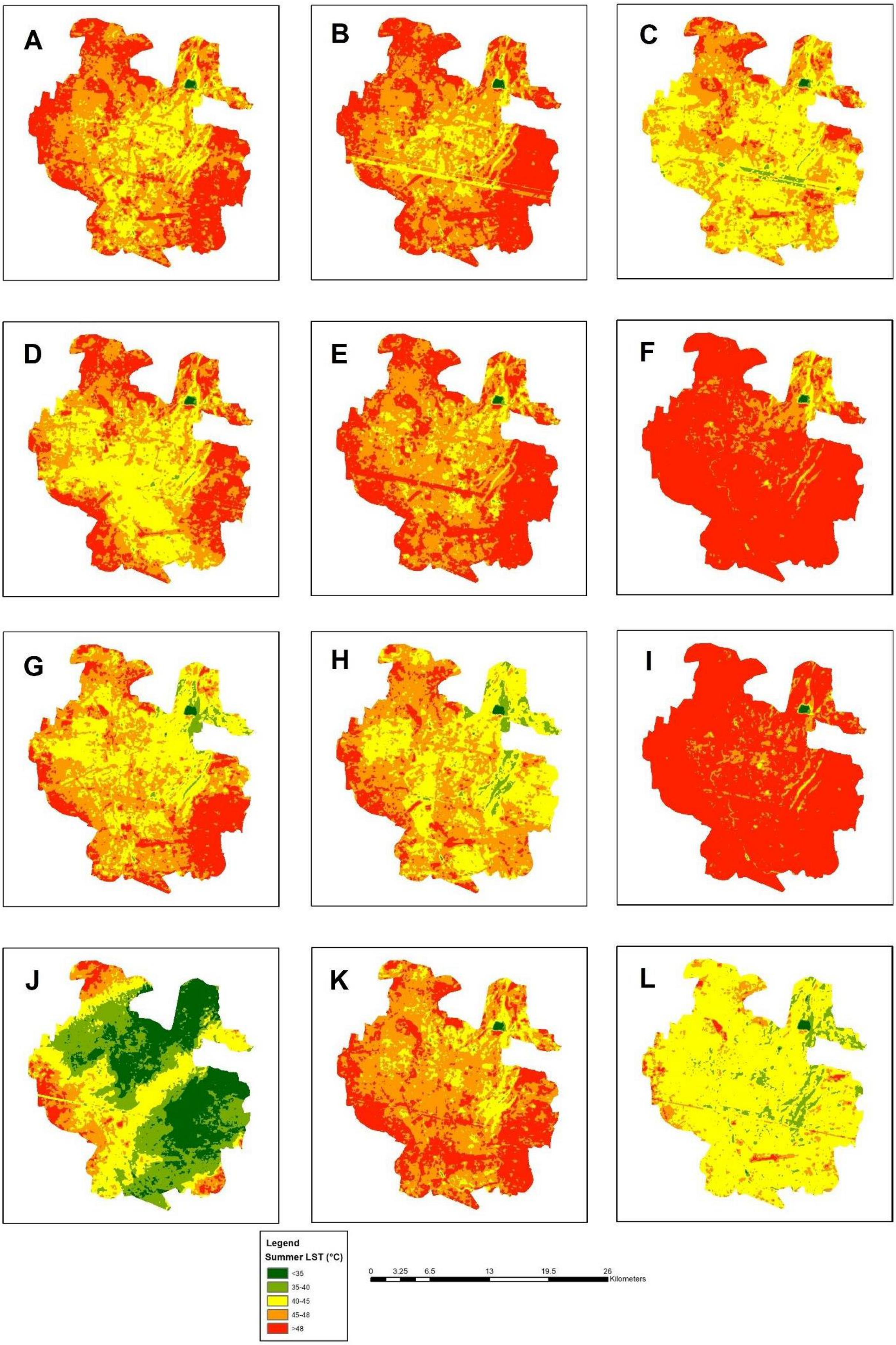

Figure 14 Summer LST distribution in the study area (2014-2025).

3.4 Classified Winter LST Area Distribution (2014-2025)

Winter LST classification demonstrates episodic dominance of extreme heat categories (Table 7) (Figure 15). In 2016, Class 5 (Above 28°C) covered 360.91 km^2 (95.93%), representing the most thermally intense winter within the study period. In contrast, 2019 exhibited a dominance of Class 2 (18-22°C) (214.56 km^2; 57.03%), indicating a cooler distribution. Post-2020 winters show mixed behavior. In 2025, Class 4 (25-28°C) expanded to 296.13 km^2 (78.71%), while Class 5 (Above 28°C) reduced to 48.01 km^2 (12.76%). Winter distribution is more variable than summer, reflecting sensitivity to atmospheric conditions.

Table 7 Winter LST class area (km^2 and %), 2014-2025.

Year	**Below 18°C**		**18-22°C**		**22-25°C**		**25-28°C**		**Above 28°C**	
	km^2	**%**	**km^2**	**%**	**km^2**	**%**	**km^2**	**%**	**km^2**	**%**
2014	0.04	0.01	15.74	4.18	47.36	12.59	107.71	28.63	205.36	54.59
2015	0.00	0.00	0.38	0.10	0.93	0.25	59.39	15.79	315.52	83.87
2016	0.00	0.00	0.29	0.08	0.71	0.19	14.31	3.80	360.91	95.93
2017	0.00	0.00	0.88	0.24	7.31	1.94	186.43	49.55	181.58	48.27
2018	0.00	0.00	4.41	1.17	37.67	10.01	237.71	63.18	96.43	25.63
2019	118.90	31.60	214.56	57.03	41.61	11.06	1.15	0.31	0.00	0.00
2020	1.69	0.45	37.91	10.08	32.18	8.55	172.76	45.92	131.67	35.00
2021	0.00	0.00	6.55	1.74	76.38	20.30	234.05	62.21	59.23	15.74
2022	0.00	0.00	0.92	0.24	14.82	3.94	265.05	70.45	95.43	25.37
2023	0.00	0.00	1.07	0.28	66.61	17.71	241.26	64.13	67.27	17.88
2024	0.00	0.00	0.50	0.13	3.37	0.90	149.11	39.63	223.24	59.34
2025	0.00	0.00	1.05	0.28	31.02	8.25	296.13	78.71	48.01	12.76

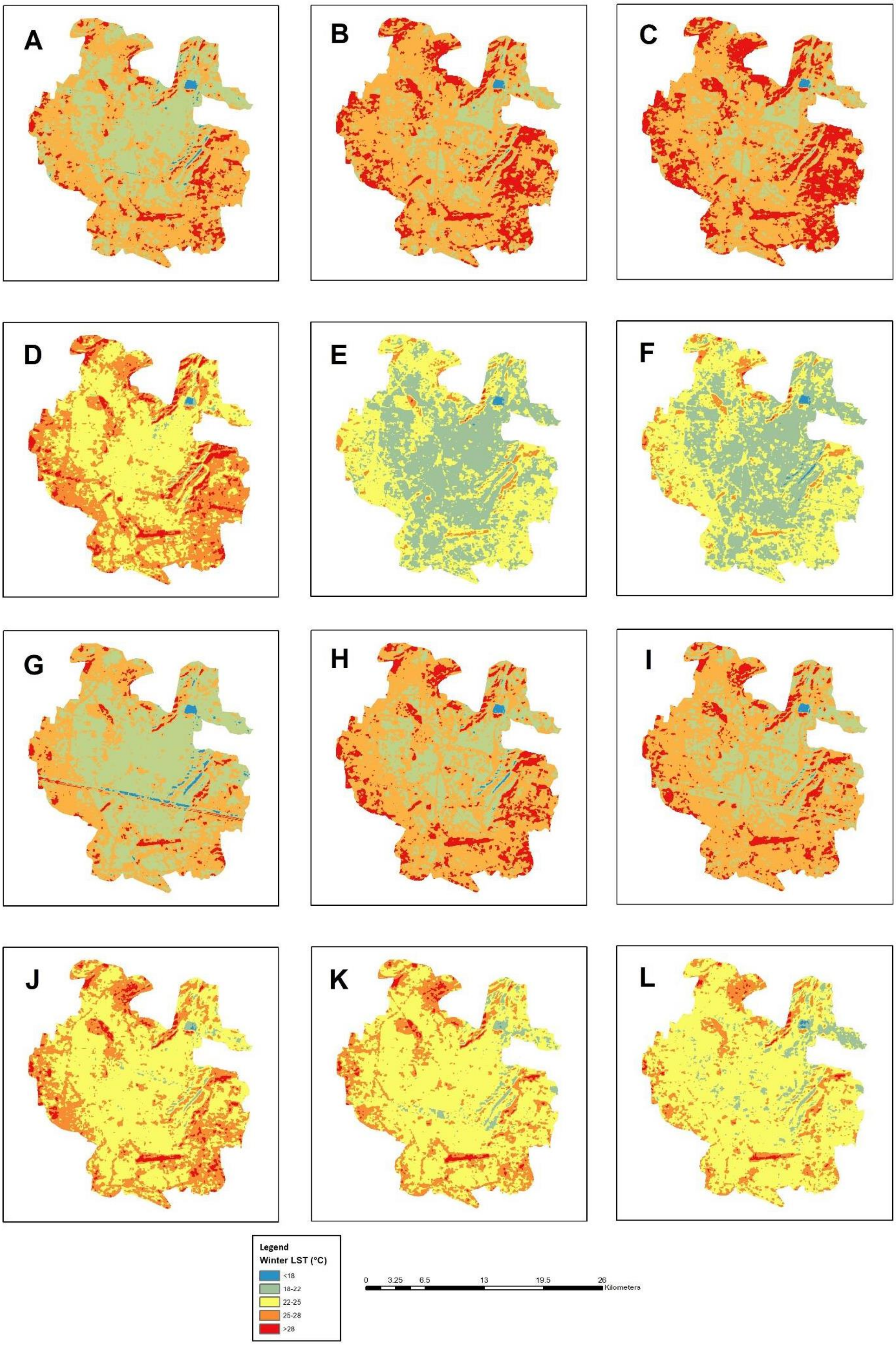

Figure 15 Winter LST distribution in the study area (2014-2025).

Minimal representation of Class 1 (Below 18°C) across most winters indicates limited cold-surface presence within the built-up boundary.

3.5 Classified Summer UTFVI Area Distribution (2014-2025)

Summer UTFVI classes indicate persistent ecological stress (Table 8) (Figure 16). Class 5 (Very strong) ranged from 128.35 km^2 (34.12%) in 2016 to 172.04 km^2 (45.73%) in 2023. In 2019, it covered 144.62 km^2 (38.44%). Class 1 (no stress) consistently occupied more than 46% of the total area, reaching 53.98% in 2022. The coexistence of high stress and no-stress zones indicates spatial heterogeneity within the urban fabric. UTFVI patterns closely follow LST intensity zones, consistent with earlier UTFVI applications in Indian cities.

Table 8 Area (km^2) and percentage (%) distribution of summer UTFVI classes (1-5) for 2014-2025.

Year	No stress		Weak		Moderate		Strong		Very strong	
	km^2	%	km^2	%	km^2	%	km^2	%	km^2	%
2014	197.72	52.56	12.51	3.32	12.46	3.31	12.10	3.22	141.43	37.59
2015	198.23	52.69	12.07	3.21	11.65	3.10	11.57	3.08	142.69	37.93
2016	198.17	52.67	17.53	4.66	16.77	4.46	15.41	4.10	128.35	34.12
2017	202.63	53.86	9.70	2.58	9.54	2.54	9.37	2.49	144.97	38.53
2018	199.74	53.09	12.06	3.21	11.94	3.17	11.67	3.10	140.80	37.43
2019	191.66	50.94	13.50	3.59	13.41	3.57	13.02	3.46	144.62	38.44
2020	202.01	53.70	13.64	3.63	12.78	3.40	11.77	3.13	136.01	36.15
2021	175.65	46.69	16.11	4.28	16.44	4.37	16.25	4.32	151.78	40.34
2022	203.07	53.98	13.97	3.71	13.15	3.49	12.82	3.41	133.21	35.41
2023	176.39	46.88	8.64	2.30	9.42	2.50	9.73	2.59	172.04	45.73
2024	197.03	52.37	14.29	3.80	13.81	3.67	13.08	3.48	138.01	36.68
2025	199.21	52.95	16.11	4.28	15.91	4.23	14.93	3.97	130.04	34.57

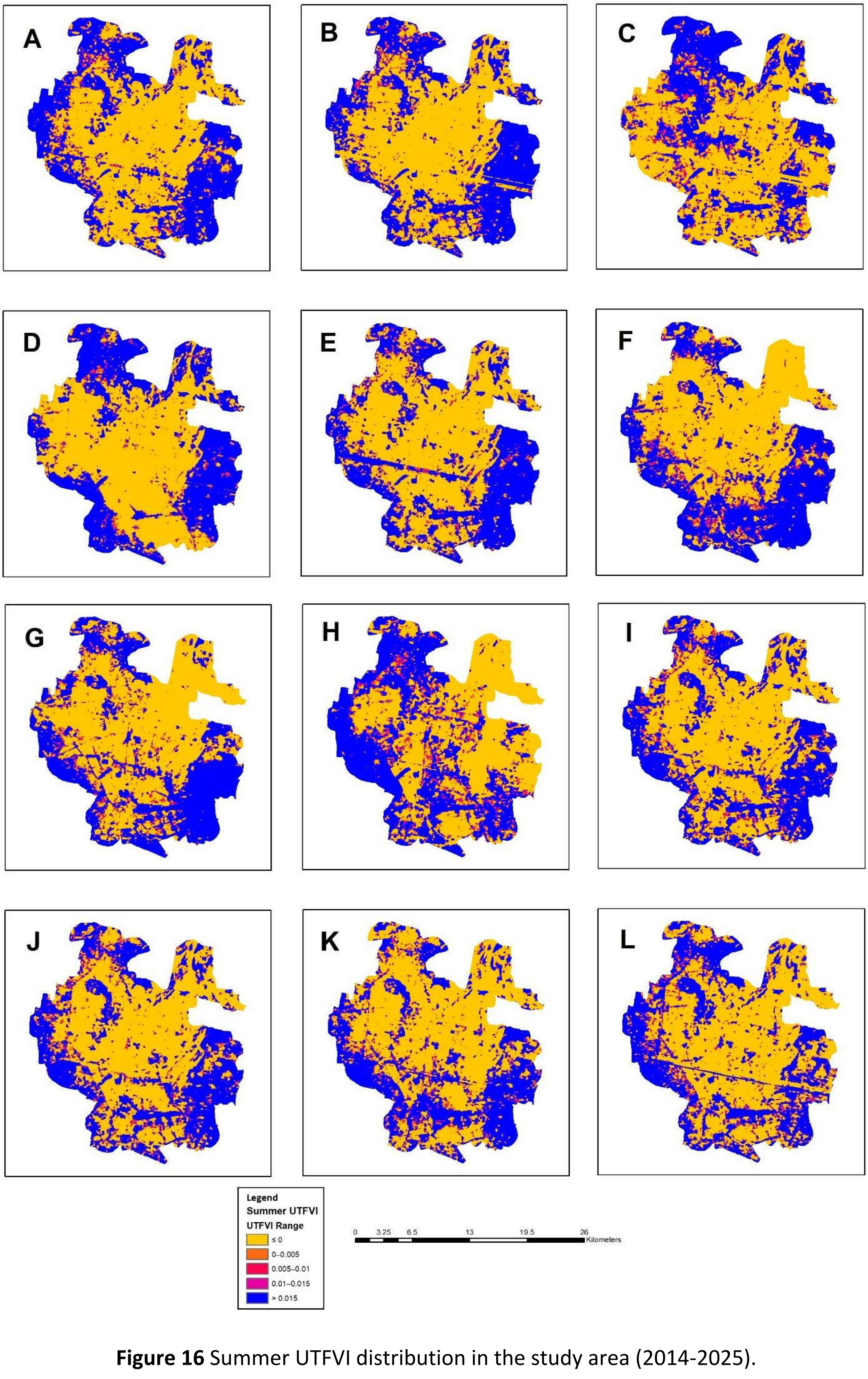

Figure 16 Summer UTFVI distribution in the study area (2014-2025).

3.6 Classified Winter UTFVI Area Distribution (2014-2025)

Winter UTFVI exhibits greater fluctuation than summer (Table 9) (Figure 17). The maximum Class 5 coverage occurred in 2019, at 218.69 km^2 (58.13%). Elevated stress also occurred in 2020, covering 185.71 km^2 (49.36%). By 2025, Class 5 declined to 120.92 km^2 (32.14%).

Table 9 Area (km^2) and percentage (%) distribution of winter UTFVI classes (1-5) for 2014-2025.

Year	No stress		Weak		Moderate		Strong		Very strong	
	km²	%	km²	%	km²	%	km²	%	km²	%
2014	174.67	46.43	7.44	1.98	7.61	2.02	7.44	1.98	179.06	47.60
2015	202.22	53.75	9.43	2.51	9.31	2.47	9.01	2.40	146.24	38.87
2016	202.19	53.74	10.48	2.79	10.26	2.73	9.68	2.57	143.62	38.17
2017	201.94	53.68	9.44	2.51	9.38	2.49	9.07	2.41	146.38	38.91
2018	201.91	53.67	10.76	2.86	10.35	2.75	9.86	2.62	143.34	38.10
2019	147.68	39.25	3.10	0.82	3.28	0.87	3.47	0.92	218.69	58.13
2020	159.10	42.29	10.70	2.84	10.49	2.79	10.22	2.72	185.71	49.36
2021	175.40	46.62	14.50	3.85	13.74	3.65	13.13	3.49	159.44	42.38
2022	208.35	55.38	13.40	3.56	12.40	3.30	12.28	3.26	129.79	34.50
2023	204.65	54.40	11.29	3.00	10.87	2.89	10.62	2.82	138.79	36.89
2024	206.32	54.84	13.40	3.56	13.04	3.47	12.46	3.31	131.00	34.82
2025	211.68	56.27	15.61	4.15	14.40	3.83	13.62	3.62	120.92	32.14

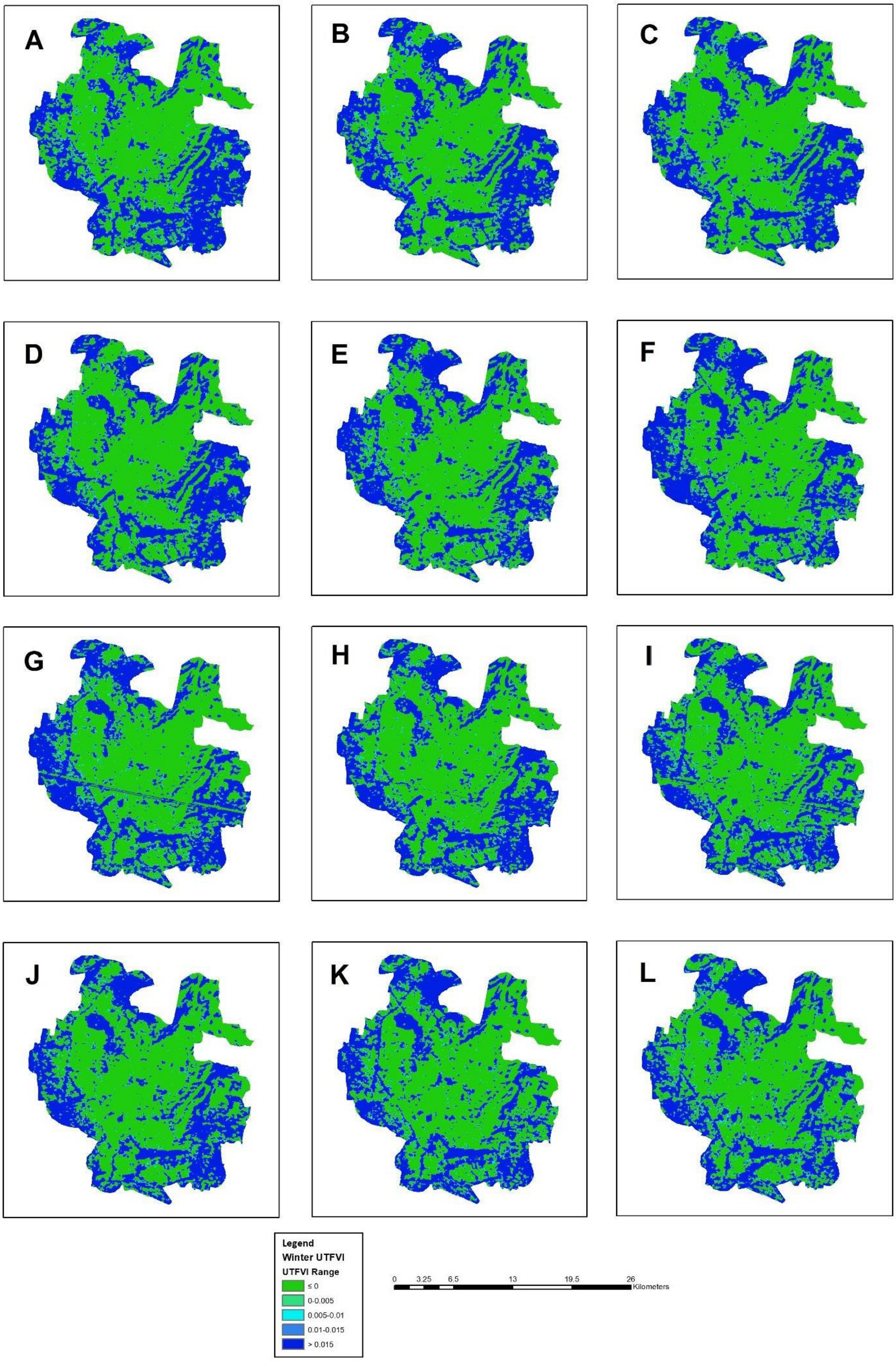

Figure 17 Winter UTFVI distribution in the study area (2014-2025).

Class 1, a No-stress class, frequently exceeded 50% of the area in 2022 and 2025, which indicates stronger spatial cooling in certain winters. The contrast between winter 2016, which shows extreme LST dominance, and winter 2019, which reflects high UTFVI stress, highlights the importance of relative thermal deviation and not absolute temperature alone.

The spatial distribution of UTFVI provides a clearer representation of ecological thermal stress than the mean value does. Although the average UTFVI remained close to zero in all years, the classified maps reveal persistent concentrations of strong and very strong stress within the urban core. In contrast, no-stress zones remained associated with vegetated and peripheral areas. This spatial heterogeneity indicates that ecological pressure is not uniformly distributed across Jaipur but is concentrated in specific urban environments where thermal conditions remain consistently elevated.

3.7 Maximum and Minimum UTFVI Intensity

Although the mean UTFVI is approximately zero, extreme values indicate the intensity of ecological stress. Summer maximum stress peaked in 2019 and 2023. The data show that winter maximum stress peaked in 2019. The minimum values remained negative throughout, indicating relative cooling zones associated with vegetation and peri-urban surfaces.

The persistent presence of Class 5 (Very Strong Stress) across all years confirms structural thermal stress within the urban system in the study area. The magnitude and spatial continuity of stress zones align with established relationships between surface temperature, built-up density, and ecological degradation.

4. Discussion

4.1 Long-Term Seasonal Thermal Behaviour (2014-2025)

The seasonal LST pattern shows clear year-to-year variability rather than a steady warming trend. The summer mean LST ranged from 41.23°C in 2023 to 50.62°C in 2019, reflecting the combined influence of climatic variability and land surface characteristics. Similarly, the winter mean LST varied from 19.01°C in 2019 to 30.81°C in 2016, indicating substantial interannual fluctuations in seasonal thermal behaviour. The exceptionally high summer temperatures observed in 2019 and the elevated winter temperatures in 2016 may also be associated with large-scale meteorological variability in addition to local surface conditions. Previous studies have reported that warmer and drier atmospheric conditions linked to large-scale climate variability, including El Niño events, can intensify summer thermal extremes. At the same time, variations in western disturbances influence winter temperature anomalies across northwestern India [45, 46]. Although the present study does not explicitly analyse meteorological datasets, these processes provide a plausible climatic context for interpreting the observed seasonal anomalies. The regression results show weak slopes, indicating no pronounced linear warming trend over the study period [47]. Similar behaviour has been observed in other Indian cities, where LST responds more strongly to rainfall variability and land-cover change than to gradual warming [48]. Guha et al. [8] also reported that LST-land-cover relationships vary seasonally, with impervious surfaces exerting greater influence during summer, whereas atmospheric conditions play a comparatively larger role during winter.

The temporal regression analysis presented in this study was intended to summarise the overall direction of seasonal LST variability rather than to characterise long-term climatic trends. Urban thermal environments are influenced by interannual meteorological variability, seasonal rainfall, atmospheric circulation, and land-surface characteristics, which can produce nonlinear responses not fully captured by simple linear regression. Therefore, the weak regression relationships observed in this study should be interpreted as indicating the absence of a pronounced linear trend over the study period rather than the absence of climatic variability.

The high-temperature classes dominated in 2014 and 2019, when Class 5 covered more than 75% of the area this indicated persistent heat storage in dense urban zones. Built-up materials retain heat, especially during dry pre-monsoon conditions. Yuan and Bauer [6] showed that impervious surfaces are a stronger control on urban heat intensity than vegetation, which aligns with these results. The winter patterns are less consistent across the study area. The 2016 case, with 95.93% of the area under Class 5, suggests short-term intensification under stable atmospheric conditions. Reduced mixing during winter can enhance urban heat intensity [1]. Jaipur shows persistent summer heat linked to its urban structure, while winter behaviour remains more episodic.

4.2 Anthropogenic Radiance Growth and Its Thermal Implications

The VIIRS radiance increased from about 19 units in 2014 to 26.57 units in 2025, indicating steady urban expansion across the study region. The strong regression fit (R^2 = 0.86) confirms this upward trend. Earlier studies have shown that VIIRS radiance is a reliable proxy for built-up growth and economic activity [22, 49], and can capture urban change at finer scales [17]. Its relationship with seasonal LST remains weak to moderate. The negative association with summer LST suggests that higher radiance does not directly translate into higher surface temperature. Similar patterns have been reported in other cities [8].

The observed divergence between the increase in nighttime radiance and seasonal LST reflects the operation of multiple physical processes rather than a direct causal relationship. Nighttime radiance primarily represents the spatial intensity of anthropogenic activity, whereas land surface temperature is controlled by the surface energy balance. Impervious materials such as concrete and asphalt possess high heat storage capacity and release thermal energy gradually, while vegetated surfaces reduce surface temperature through evapotranspiration and shading. In addition, seasonal variations in soil moisture, atmospheric humidity, and wind circulation influence the partitioning of sensible and latent heat, resulting in different thermal responses under similar levels of urban activity. Consequently, areas exhibiting comparable nighttime radiance may display different surface temperatures depending on their land-surface characteristics and prevailing environmental conditions [21].

In addition to vegetation and seasonal climatic variability, differences in urban construction materials may also contribute to the observed thermal response. Highly developed urban areas increasingly incorporate reflective roofing materials, improved building envelopes, and other climate-responsive construction practices that can reduce surface heat absorption despite high levels of anthropogenic activity. Although the present study does not evaluate roofing materials or building characteristics directly, these factors provide a plausible explanation for the relatively weak association between nighttime radiance and summer LST and have been widely recognised as effective measures for mitigating urban heat.

The observed weak association between nighttime radiance and seasonal LST suggests that anthropogenic activity alone does not govern the thermal behaviour of Jaipur. Nighttime radiance primarily represents the intensity of human activity and illuminated infrastructure. In contrast, land surface temperature is additionally influenced by surface materials, vegetation cover, surface moisture, urban geometry, and seasonal atmospheric conditions. Consequently, areas with similar radiance levels may exhibit different thermal responses depending on their local environmental characteristics. The observed decoupling therefore reflects the combined influence of urban surface composition and seasonal climatic variability rather than a direct one-to-one relationship between anthropogenic radiance and surface temperature.

4.3 Seasonal Contrast in Classified Heat Expansion

The classified LST maps show that extreme summer heat (Class 5) consistently occupies large areas. In 2019, it reached 85.57%, while in 2023 it shifted towards moderate Class 3 (55.32%), indicating the role of seasonal conditions in shaping heat distribution.

Similar patterns have been observed in other Asian cities, where heat zones expand during dry years and contract during wetter years [50]. Jaipur follows this trend with moderate classes increasing when moisture reduces surface heating. The winter patterns are more variable across Jaipur. The 2016 anomaly contrasts with 2019, when Class 2 dominated (57.03%), suggesting that winter heat does not follow a fixed trend and is likely influenced by atmospheric factors such as western disturbances and wind conditions. Despite this variability, the high summer classes remain consistent, indicating that the built-up core maintains elevated temperatures.

The classified LST and UTFVI maps consistently demonstrate that persistent high-temperature and high-stress zones remain concentrated within the urban core throughout the study period. In contrast, comparatively lower thermal classes are primarily distributed towards the vegetated and peripheral parts of Jaipur. Although a dedicated LULC analysis was beyond the scope of the present study, the observed spatial patterns are consistent with the well-established relationship between urban built-up environments, reduced vegetation cover, and elevated land surface temperatures reported in previous studies. Therefore, the thermal maps presented in this study provide an appropriate basis for interpreting the spatial evolution of urban heat without requiring a separate land-use classification.

4.4 Ecological Stress Dynamics Based on UTFVI

The UTFVI reflects ecological stress rather than absolute temperature. In Jaipur, summer Class 5 ranged from 34% to 46% of the area, while winter values peaked at 58.13% in 2019, indicating that a large part of the city experiences severe thermal stress. Previous studies have linked high UTFVI values with dense built-up areas and reduced groundwater recharge [10, 11], and similar patterns are evident in central Jaipur. The coexistence of low (Class 1) and high (Class 5) categories highlights strong intra-urban contrast in Jaipur. The Vegetated and peri-urban areas consistently act as cooling zones, which support green cover to reduce heat [51-53]. The persistence of high-UTFVI zones reflects the ecological stress that remains structurally embedded, even when the mean LST fluctuates. The spatial distribution of the “No Stress” and lower UTFVI classes is predominantly observed along the peripheral areas of Jaipur, particularly towards the Aravalli hill ranges. The relatively lower thermal stress in these locations is likely associated with higher vegetation cover, comparatively lower development intensity, and the moderating influence of the surrounding natural landscape. Although the present study does not quantify the specific cooling contribution of the Aravalli hills, the observed spatial pattern is consistent with previous studies reporting that natural topography and vegetated landscapes surrounding urban areas contribute to mitigating local thermal stress and improving ecological thermal conditions [54].

The interpretation of UTFVI should therefore focus primarily on the spatial persistence and expansion of stress classes rather than on mean annual values. Because UTFVI represents a relative thermal deviation from the seasonal mean, average values remain close to zero by definition and provide limited ecological insight. In contrast, the classified UTFVI maps effectively identify persistent hotspots and cooling zones, allowing a more meaningful assessment of intra-urban ecological stress and thermal heterogeneity.

4.5 Integrated Interpretation of Thermal and Radiance Dynamics

The combined analysis shows a clear pattern across the study area. The radiance increased steadily from 2014 to 2025, confirming ongoing urban expansion. In contrast, the seasonal LST fluctuated within a defined range without a linear increase. Despite this, the high-temperature classes and UTFVI stress zones remained spatially persistent. This divergence indicates that urban growth alone does not control surface temperature. Land cover, vegetation, impervious surfaces, and seasonal atmospheric conditions shape LST. Similar behaviour has been reported in other Indian cities [55, 56]. Integrating continuous and classified data improves interpretation. The mean LST and radiance capture long-term trends, while the classified LST and UTFVI reveal the spatial concentration of heat and stress. This whole approach provides a more complete understanding of urban thermal behaviour. This behaviour indicates that increasing anthropogenic activity does not necessarily produce a proportional increase in surface temperature, particularly where local surface characteristics and seasonal environmental conditions regulate heat storage and dissipation. These findings demonstrate that anthropogenic radiance should not be interpreted as a direct indicator of urban thermal intensity. Instead, nighttime radiance reflects the level of urban development and human activity. In contrast, the thermal response depends on the interaction of land-cover composition, the heat-strorage properties of urban materials, vegetation cooling, and seasonal meteorological conditions. This interaction explains why persistent growth in nighttime radiance was accompanied by comparatively weak temporal changes in seasonal LST across the study period. The spatial persistence of thermal hotspots identified in this study provides a practical basis for prioritising future heat mitigation measures in areas experiencing sustained ecological thermal stress.

5. Conclusion

Seasonal land surface temperature, ecological stress, and nighttime radiance are assessed in this study of Jaipur for the period 2014-2025 using harmonised Landsat-8 and VIIRS datasets, and are analysed in Google Earth Engine. The analysis combined continuous mean indicators, regression modelling, and classified spatial expansion. This provides both temporal and spatial perspectives of urban thermal dynamics in Jaipur. During the study period in Jaipur, the mean summer LST ranged from 41.23°C to 50.62°C while the winter LST ranged from 19.01°C to 30.81°C. The regression results showed weak linear relationships between year and seasonal LST in Jaipur. The surface temperature behaviour is characterised by interannual variability rather than steady warming, as indicated by the regression results. Based on observations from other Indian cities, this pattern seems consistent, with seasonal LST strongly influenced by land-cover arrangement and climatic variability rather than by just simple temporal progression [57]. The absence of monotonic warming indicates no thermal constancy, whereas the seasonal factors cause temperature fluctuations within an already heat-prone urban surface. The VIIRS nighttime radiance increased steadily from 19.06 to 26.57 $nW \cdot cm^{-2} \cdot sr^{-1}$, with a strong regression fit. This result supports sustained urban intensification and expansion of illuminated infrastructure in Jaipur. The similar upward trajectories in nighttime radiance have been extensively interpreted as indicators of economic growth and built-up expansion [1, 21, 27]. The statistical association between radiance and seasonal LST is weak, indicating that anthropogenic light intensity alone does not determine daytime surface heating. The surface thermal response remains mediated by a few observed factors, including vegetation fraction, impervious surface coverage, surface albedo, and seasonal atmospheric conditions [58]. The complexity of urban thermal systems in semi-arid environments leads to divergence between steady radiance growth and variable LST behaviour.

The persistent dominance of high-temperature classes during extreme summers is evident in the results from LST classification in Jaipur. Class 5 (>48°C) occupied more than 75% of the total area in 2019, indicating widespread extreme heat conditions in Jaipur. The winter heat expansion was episodic rather than continuous in 2016, indicating a pronounced irregularity in which high-temperature classes dominated nearly the entire urban area of the study region. These findings reinforce that summer heat stress in Jaipur is structurally embedded within the built-up core. The amplification of winter heat is more climate-sensitive.

The UTFVI results also showed that ecological stress remains a consistent feature across the city. The areas classified as strong stress covered more than one-third of the urban area in most seasons and in some years exceeded 45%. Similar patterns have been reported in other rapidly growing cities where high stress zones usually coincide with dense built-up areas and limited vegetation cover [58, 59]. In years when the average LST was slightly lower, the stress zones did not disappear. They remained concentrated in particular parts of the city, showing clear temperature differences within the urban area. The combined results indicate that urban growth and surface temperature are related but not always directly proportional. The Nighttime radiance clearly shows increasing human activity and expansion of the city. The LST and UTFVI reveal where heat is actually concentrated and where ecological stress is strongest. Jaipur's urban structure and land-surface characteristics maintain thermal pressure even when short-term climatic conditions vary due to the continued dominance of high summer temperature classes and strong stress zones.

From a planning perspective, the findings indicate that heat mitigation strategies should prioritise areas exhibiting persistently high temperatures and high UTFVI classes identified in this study, rather than applying uniform city-wide interventions. Priority should be given to preserving existing green spaces, increasing urban tree cover within densely developed neighbourhoods, promoting climate-responsive building materials and cool roofing practices, and incorporating green infrastructure into future urban development. These targeted measures are expected to improve local thermal resilience while supporting sustainable urban planning in rapidly expanding semi-arid cities. Future research should incorporate high-resolution land cover mapping and in situ microclimatic observations to better resolve intra-urban heterogeneity. The integration of multi-sensor datasets with process-based urban climate modelling would further clarify the interaction between anthropogenic expansion and surface thermal dynamics. The current study provides an integrated framework that combines continuous assessment of radiance growth with classified analyses of thermal and ecological stress. This approach is suitable for monitoring long-term urban heat dynamics in semi-arid metropolitan environments. It contributes empirical evidence to ongoing discussions on urban expansion, surface temperature variability, and ecological resilience.

Acknowledgments

The author acknowledges the availability of open-access geospatial datasets from the United States Geological Survey (USGS) for Landsat 8 surface temperature data and from the National Oceanic and Atmospheric Administration (NOAA) for VIIRS nighttime radiance data. The study also utilised computational resources available through Google Earth Engine. The open spatial datasets from national and international agencies including the Survey of India and the Indian Space Research Organisation (ISRO) which supported boundary delineation and spatial referencing. These publicly accessible data platforms made the analysis possible for the study area of Jaipur.

Author Contributions

R.K.G. developed the initial concept for this article and provided comprehensive editing and oversight throughout the process. Y.K.T. was responsible for data acquisition, Google Earth Engine scripting, data processing, statistical analysis, and ensuring accuracy and relevance. G.Y. & A.G. prepared the initial draft and executed the necessary computations while validating the analytical methods employed in this research. S.G. explored specific approaches and reviewed and approved the final version of the manuscript.

Funding

This research received no external funding.

Competing Interests

The authors declares that there are no competing interests.

Data Availability Statement

All the datasets used in the current study are publicly available. The Landsat 8 Collection 2 Level-2 data were obtained from the United States Geological Survey archive using their official website. The VIIRS Day/Night Band monthly radiance data were accessed from the NOAA data repository. All the image processing and statistical analysis were performed using Google Earth Engine and SPSS software.

AI-Assisted Technologies Statement

Grammarly software was used only for language editing to improve grammar and clarity. This does not contribute to research design, data processing, analysis, interpretation and scientific writing. All the components of the study including methodology, coding, statistical analysis, and manuscript preparation were carried out independently by the author. The author accepts full responsibility for the accuracy and integrity of the work.

References

1. Voogt JA, Oke TR. Thermal remote sensing of urban climates. Remote Sens Environ. 2003; 86: 370-384.
2. Roy DP, Wulder MA, Loveland TR, Ce W, Allen RG, Anderson MC, et al. Landsat-8: Science and product vision for terrestrial global change research. Remote Sens Environ. 2014; 145: 154-172.
3. Qin Z, Karnieli A, Berliner P. A mono-window algorithm for retrieving land surface temperature from Landsat TM data and its application to the Israel-Egypt border region. Int J Remote Sens. 2001; 22: 3719-3746.
4. Li ZL, Tang BH, Wu H, Ren H, Yan G, Wan Z, et al. Satellite-derived land surface temperature: Current status and perspectives. Remote Sens Environ. 2013; 131: 14-37.
5. Chander G, Markham BL, Helder DL. Summary of current radiometric calibration coefficients for Landsat MSS, TM, ETM+, and EO-1 ALI sensors. Remote Sens Environ. 2009; 113: 893-903.
6. Yuan F, Bauer ME. Comparison of impervious surface area and normalized difference vegetation index as indicators of surface urban heat island effects in Landsat imagery. Remote Sens Environ. 2007; 106: 375-386.
7. Nimish G, Bharath HA, Lalitha A. Exploring temperature indices by deriving relationship between land surface temperature and urban landscape. Remote Sens Appl. 2020; 18: 100299.
8. Guha S, Govil H, Gill N, Dey A. A long-term seasonal analysis on the relationship between LST and NDBI using Landsat data. Quat Int. 2021; 575: 249-258.
9. Wang H, Zhang Y, Tsou JY, Li Y. Surface urban heat island analysis of Shanghai (China) based on the change of land use and land cover. Sustainability. 2017; 9: 1538.
10. Moisa MB, Gemeda DO. Assessment of urban thermal field variance index and thermal comfort level of Addis Ababa metropolitan city, Ethiopia. Heliyon. 2022; 8: e10185.
11. Moharir KN, Pande CB, Gautam VK, Tolche AD, Sharma C, Othman K, et al. Investigation of urban heat island and urban thermal field variance index effect on groundwater level in India using Google Earth Engine. J Water Clim Change. 2025; 16: 2974-2999.
12. Gupta RK. Spatial dynamics of micro-urban heat islands and satellite-derived indices of Ahmedabad City, India. J Earth Syst Sci. 2025; 134: 23.
13. Gupta R. GIS-based analysis of land surface characteristics and urban heat islands in metropolitan cities of India. Int J Eng Geosci. 2025; 10: 440-455.
14. Miller SD, Mills SP, Elvidge CD, Lindsey DT, Lee TF, Hawkins JD. Suomi satellite brings to light a unique frontier of nighttime environmental sensing capabilities. Proc Natl Acad Sci. 2012; 109: 15706-15711.
15. Elvidge CD, Baugh K, Zhizhin M, Hsu FC, Ghosh T. VIIRS night-time lights. Int J Remote Sens. 2017; 38: 5860-5879.
16. Chen X, Nordhaus WD. VIIRS nighttime lights in the estimation of cross-sectional and time-series GDP. Remote Sens. 2019; 11: 1057.
17. Bennett MM, Smith LC. Advances in using multitemporal night-time lights satellite imagery to detect, estimate, and monitor socioeconomic dynamics. Remote Sens Environ. 2017; 192: 176-197.

18. Uprety S, Cao C, Gu Y, Shao X, Blonski S, Zhang B. Calibration improvements in S-NPP VIIRS DNB sensor data record using version 2 reprocessing. IEEE Trans Geosci Remote Sens. 2019; 57: 9602-9611.
19. Chen Z, Yu B, Yang C, Zhou Y, Yao S, Qian X, et al. An extended time series (2000-2018) of global NPP-VIIRS-like nighttime light data from a cross-sensor calibration. Earth Syst Sci Data. 2021; 13: 889-906.
20. Coesfeld J, Kuester T, Kuechly HU, Kyba CC. Reducing variability and removing natural light from nighttime satellite imagery: A case study using the VIIRS DNB. Sensors. 2020; 20: 3287.
21. Li X, Ma R, Zhang Q, Li D, Liu S, He T, et al. Anisotropic characteristic of artificial light at night-Systematic investigation with VIIRS DNB multi-temporal observations. Remote Sens Environ. 2019; 233: 111357.
22. Zhao M, Zhou Y, Li X, Cao W, He C, Yu B, et al. Applications of satellite remote sensing of nighttime light observations: Advances, challenges, and perspectives. Remote Sens. 2019; 11: 1971.
23. Song J, Wang J, Xia X, Lin R, Wang Y, Zhou M, et al. Characterization of urban heat islands using city lights: Insights from MODIS and VIIRS DNB observations. Remote Sens. 2021; 13: 3180.
24. Liu K, Su H, Zhang L, Yang H, Zhang R, Li X. Analysis of the urban heat island effect in Shijiazhuang, China using satellite and airborne data. Remote Sens. 2015; 7: 4804-4833.
25. Olgun R, Karakuş N, Selim S, Yilmaz T, Erdoğan R, Aklıbaşında M, et al. Impacts of landscape composition on land surface temperature in expanding desert cities: A case study in Arizona, USA. Land. 2025; 14: 1274.
26. Berg E, Kucharik C. The dynamic relationship between air and land surface temperature within the Madison, Wisconsin urban heat island. Remote Sens. 2021; 14: 165.
27. Foga S, Scaramuzza PL, Guo S, Zhu Z, Dilley Jr RD, Beckmann T, et al. Cloud detection algorithm comparison and validation for operational Landsat data products. Remote Sens Environ. 2017; 194: 379-390.
28. Liang S, Xu D, Wang P, Zhang M. Study on the impact of land use and climate change on the spatiotemporal evolution of NDVI in Tianjin, China. Pol J Environ Stud. 2025. doi: 10.15244/pjoes/208254.
29. Zhang M. A global perspective on urban thermal environment: From satellite data to sustainable development. Cell Rep Sustain. 2025; 2: 100522.
30. Cao C, Bai Y. Quantitative analysis of VIIRS DNB nightlight point source for light power estimation and stability monitoring. Remote Sens. 2014; 6: 11915-11935.
31. Liu Y, Yu P, Wang H, Peng J, Yu Y. Ten years of VIIRS land surface temperature product validation. Remote Sens. 2022; 14: 2863.
32. Wang X, Key JR, Moeller S, Dworak RJ, Shao X, Knapp KR. Extending AVHRR climate data records into the VIIRS era for polar climate research. Remote Sens. 2025; 17: 3495.
33. Jiao Z, Mu X. Estimating global instantaneous near-surface air temperature from clear-sky Landsat 8/9 observations using ensemble machine learning. Remote Sens. 2026; 18: 1885.
34. Adiguzel AD, Zhang M, Kaya AY, Karadeniz E, Mantas S. Projecting tourism climate suitability in Türkiye under climate change scenarios: Insights from the summer simmer index. Adv Space Res. 2026; 77: 8939-8955.
35. Li H, Sun D, Yu Y, Wang H, Liu Y, Liu Q, et al. Evaluation of the VIIRS and MODIS LST products in an arid area of Northwest China. Remote Sens Environ. 2014; 142: 111-121.

36. Guillevic PC, Biard JC, Hulley GC, Privette JL, Hook SJ, Olioso A, et al. Validation of land surface temperature products derived from the visible infrared imaging radiometer suite (VIIRS) using ground-based and heritage satellite measurements. Remote Sens Environ. 2014; 154: 19-37.
37. Zhang J, Jaker SL, Reid JS, Miller SD, Solbrig J, Toth TD. Characterization and application of artificial light sources for nighttime aerosol optical depth retrievals using the visible infrared imager radiometer suite day/night band. Atmos Meas Tech. 2019; 12: 3209-3222.
38. Xia L, Mao K, Ma Y, Zhao F, Jiang L, Shen X, et al. An algorithm for retrieving land surface temperatures using VIIRS data in combination with multi-sensors. Sensors. 2014; 14: 21385-21408.
39. Duan SB, Li ZL, Tang BH, Wu H, Tang R. Generation of a time-consistent land surface temperature product from MODIS data. Remote Sens Environ. 2014; 140: 339-349.
40. Sobrino JA, Sòria G, Prata AJ. Surface temperature retrieval from along track scanning radiometer 2 data: Algorithms and validation. J Geophys Res. 2004; 109. doi: 10.1029/2003JD004212.
41. Sobrino JA, Jiménez-Muñoz JC. Land surface temperature retrieval from thermal infrared data: An assessment in the context of the surface processes and ecosystem changes through response analysis (SPECTRA) mission. J Geophys Res. 2005; 110. doi: 10.1029/2004JD005588.
42. Pérez Díaz C, Lakhankar T, Romanov P, Khanbilvardi R, Yu Y. Evaluation of VIIRS land surface temperature using CREST-SAFE air, snow surface, and soil temperature data. Geosciences. 2015; 5: 334-360.
43. Islam T, Hulley GC, Malakar NK, Radocinski RG, Guillevic PC, Hook SJ. A physics-based algorithm for the simultaneous retrieval of land surface temperature and emissivity from VIIRS thermal infrared data. IEEE Trans Geosci Remote Sens. 2016; 55: 563-576.
44. Román MO, Justice C, Paynter I, Boucher PB, Devadiga S, Endsley A, et al. Continuity between NASA MODIS Collection 6.1 and VIIRS Collection 2 land products. Remote Sens Environ. 2024; 302: 113963.
45. Malakar NK, Hulley GC, Hook SJ, Laraby K, Cook M, Schott JR. An operational land surface temperature product for Landsat thermal data: Methodology and validation. IEEE Trans Geosci Remote Sens. 2018; 56: 5717-5735.
46. Hunt KM, Baudouin JP, Turner AG, Dimri AP, Jeelani G, Pooja, et al. Western disturbances and climate variability: A review of recent developments. Weather Clim Dyn. 2025; 6: 43-112.
47. Javed A, Anshuman K, Kumar P, Sachan D. The decline in western disturbance activity over Northern India in recent decades. Clim Change. 2023; 176: 97.
48. Elvidge CD, Hsu FC, Zhizhin M, Ghosh T, Sparks T. Statistical moments of VIIRS night-time lights. Int J Remote Sens. 2024; 45: 7778-7802.
49. Zhang Y, Song C, Band LE, Sun G, Li J. Reanalysis of global terrestrial vegetation trends from MODIS products: Browning or greening? Remote Sens Environ. 2017; 191: 145-155.
50. Anucharn T, Hongpradit P, Iamchuen N, Puttinaovarat S. Spatial analysis of urban expansion and energy consumption using nighttime light data: A comparative study of Google Earth Engine and traditional methods for improved living spaces. ISPRS Int J Geo-Inf. 2025; 14: 178.
51. Holzhauer SI, Franke S, Kyba CC, Manfrin A, Klenke R, Voigt CC, et al. Out of the dark: Establishing a large-scale field experiment to assess the effects of artificial light at night on species and food webs. Sustainability. 2015; 7: 15593-15616.

52. Levin N, Duke Y. High spatial resolution night-time light images for demographic and socio-economic studies. Remote Sens Environ. 2012; 119: 1-10.
53. Hsu FC, Elvidge CD, Baugh K, Zhizhin M, Ghosh T, Kroodsma D, et al. Cross-matching VIIRS boat detections with vessel monitoring system tracks in Indonesia. Remote Sens. 2019; 11: 995.
54. Ou J, Liu X, Li X, Li M, Li W. Evaluation of NPP-VIIRS nighttime light data for mapping global fossil fuel combustion CO_2 emissions: A comparison with DMSP-OLS nighttime light data. PLoS One. 2015; 10: e0138310.
55. Jiang W, He G, Long T, Guo H, Yin R, Leng W, et al. Potentiality of using Luojia 1-01 nighttime light imagery to investigate artificial light pollution. Sensors. 2018; 18: 2900.
56. Li X, Zhang R, Huang C, Li D. Detecting 2014 northern Iraq insurgency using night-time light imagery. Int J Remote Sens. 2015; 36: 3446-3458.
57. Gupta RK. Geospatial and statistical analysis of land surface temperature and land surface characteristics of Jaipur and Ahmedabad cities of India. J Geosci Environ Prot. 2024; 12: 1-19.
58. Gupta RK. Identifying urban hotspots and cold spots in Delhi using the Biophysical Landscape framework. Ecol Econ Soc. 2024; 7: 137-155.
59. Muhammad R, Zhang W, Abbas Z, Guo F, Gwiazdzinski L. Spatiotemporal change analysis and prediction of future land use and land cover changes using QGIS MOLUSCE plugin and remote sensing big data: A case study of Linyi, China. Land. 2022; 11: 419.